RANGE RESOLUTION IMPROVEMENT OF FMCW RADARS

A THESIS SUBMITTED TO
THE GRADUATE SCHOOL OF NATURAL AND APPLIED SCIENCES
OF
MIDDLE EAST TECHNICAL UNIVERSITY

BY

SİNAN KURT

IN PARTIAL FULFILLMENT OF THE REQUIREMENTS
FOR
THE DEGREE OF MASTER OF SCIENCE
IN
ELECTRICAL AND ELECTRONICS ENGINEERING

SEPTEMBER 2007

Approval of the thesis:

RANGE RESOLUTION IMPROVEMENT OF FMCW RADARS

submitted by **SİNAN KURT** in partial fulfillment of the requirements for the degree of Master of Science **in Electrical and Electronics Engineering Department, Middle East Technical University** by,

Prof. Dr. Canan ÖZGEN   _____
Dean, Graduate School of **Natural and Applied Sciences**

Prof. Dr. İsmet ERKMEN   _____
Head of Department, **Electrical and Electronics Engineering**

Assoc. Prof. Dr. Şimşek DEMİR   _____
Supervisor, **Electrical and Electronics Engineering Dept., METU**

Prof. Dr. Altunkan HIZAL   _____
Co-Supervisor, **Electrical and Electronics Engineering Dept., METU**

Examining Committee Members:

Prof. Dr. Canan TOKER   _____
Electrical and Electronics Engineering Dept., METU

Assoc. Prof. Dr. Şimşek DEMİR   _____
Electrical and Electronics Engineering Dept., METU

Prof. Dr. Altunkan HIZAL   _____
Electrical and Electronics Engineering Dept., METU

Assoc. Prof. Dr. S. Sencer KOÇ   _____
Electrical and Electronics Engineering Dept., METU

Dr. Orhan ŞENGÜL   _____
Chief Researcher, TÜBİTAK UZAY

                              Date: _____

I hereby declare that all information in this document has been obtained and presented in accordance with academic rules and ethical conduct. I also declare that, as required by these rules and conduct, I have fully cited and referenced all material and results that are not original to this work.

Name, Last name   :

Signature   :

ABSTRACT

RANGE RESOLUTION IMPROVEMENT OF FMCW RADARS

Sinan KURT

M.S., Department of Electrical and Electronics Engineering

Supervisor: Assoc. Prof. Dr. Şimşek DEMİR

Co-Supervisor: Prof. Dr. Altunkan HIZAL

September 2007, 88 pages

Frequency Modulated Continuous Wave (FMCW) radar has wide application areas in both civil and military use. The range resolution is a critical concept for these FMCW radars as for the other radar types. There are theoretical restrictions in the range resolution. In addition, the non-ideal properties of the modules used in the systems negatively affects the range resolution. The transmitter leakage, non-linear frequency sweep, FM to AM distortion and measurement errors are some of the critical non-ideal properties. The problems arising from these non-ideal properties further restrict the range resolution of FMCW radars. Another important concept for the range resolution that can be obtained from FMCW radars is the signal processing method. This thesis deals with the non-ideal properties of the system modules and techniques to reduce their effects on the range resolution. Furthermore, the signal processing methods used for FMCW radar signals and the possible improvement techniques for these methods are discussed. Moreover, a simple signal processing unit called zero crossing counter

which can be used for short range FMCW radars is implemented and range resolution performance of this zero crossing counter is investigated by carrying out measurements on a prototype FMCW radar at 2200MHz.

Keywords: FMCW radar, range resolution, transmitter leakage power, non-linear frequency sweep, zero crossing counter.

ÖZ

FMCW RADARLARDA MESAFE ÇÖZÜNÜRLÜK İYİLEŞTİRMESİ

Yüksek Lisans, Elektrik Elektronik Mühendisliği Bölümü

Tez Yöneticisi: Doç. Dr. Şimşek DEMİR

Ortak Tez Yöneticisi: Prof. Dr. Altunkan HIZAL

Eylül 2007, 88 sayfa

FMCW radar sivil ve askeri geniş uygulama alanlarına sahiptir. Diğer radar tipleri gibi FMCW radarlarda da mesafe çözünürlüğü önemli bir konudur. Mesafe çözünürlüğü için kuramsal bir sınır olduğu gibi sistemlerde kullanılan modüllerin ideal olmayan özellikleri de mesafe çözünürlüğünü kötü etkiler. Verici güç sızıntısı, doğrusal olmayan frekans taraması, frekans modülasyonu kaynaklı genlik bozulmaları ve ölçüm hataları modüllerin ideal olmayan özelliklerinin önemli sonuçlarındandır. Modüllerin bu özelliklerinden kaynaklanan sorunlar mesafe çözünürlüğünün kuramsal sınırın ötesinde kötüleşmesine sebep olur. FMCW radarlardan elde edilebilecek mesafe çözünürlüğü için bir diğer önemli konu da kullanılan işaret işleme yöntemleridir. Bu tezde sistem modüllerinin ideal olmayan özellikleri ve bu özelliklerin mesafe çözünürlüğü üzerindeki etkilerini azaltacak teknikler ele alınmıştır. Bunlarla birlikte FMCW radar işaretleri için işaret işleme yöntemleri ve bu yöntemler için mesafe çözünürlük iyileştirme teknikleri araştırılmıştır. Ayrıca kısa mesafe FMCW radarlar için kullanılan sıfır kesme sayacı adında basit bir işaret işleme ünitesi

gerçekleştirilmiştir ve 2200 MHz ana frekansında çalışan bir FMCW radar prototipi ile gerçekleştirilen ölçümler ile sıfır kesme sayacının performansı ortaya konmuştur.

Anahtar Kelimeler: FMCW radar, mesafe çözünürlük, verici sızması, doğrusal olmayan frekans taraması, sıfır kesme sayacı.

To my family

ACKNOWLEDGEMENTS

TABLE OF CONTENTS

LIST OF TABLES

LIST OF FIGURES

LIST OF ABBREVIATIONS

ARMA	Auto Regressive Moving Average
CMOS	Complementary Metal Oxide Semiconductor
CW	Continuous Wave
DAC	Digital to Analog Converter
FFEA	Fast Frequency Estimation Algorithm
FFT	Fast Fourier Transform
FMCW	Frequency Modulated Continuous Wave
IF	Intermediate Frequency
LCD	Liquid Crystal Display
LPF	Low Pass Filter
MLE	Maximum Likelihood Estimation
MUSIC	Multiple Signal Classification
PFD	Phase-Frequency Detector
PLL	Phase-Locked Loop
RMSE	Root Mean Square Error
RPC	Reflected Power Canceller
VCO	Voltage Controlled Oscillator
VT	Variable Time
ZCC	Zero Crossing Counter

CHAPTER 1

INTRODUCTION

In a radar system, detection and range calculation of a target are done by transmitting electromagnetic energy and observing the back scattered echo signal. A radar system uses either pulsed signals or continuous wave. In pulsed radars transmitted signal is a short burst of electromagnetic energy and the receiver of the system listens the echo signal after sending the transmit signal. From the echo signal, the presence of target and the time between transmitted and received signal can be calculated and time difference between the signals easily give the range information. However in continuous wave (CW) radar case, transmitter continuously sends signal therefore discrimination of transmitted signal and the echo is not the same as in pulsed radar case; there are no transmitted and received bursts of signals. To be able to obtain range information in CW radars a feasible technique, i.e. a time mark, is needed for separating the received signal from the transmitted signal and calculate the time difference between them.

In some applications, pulsed radars have more advantages on the CW radars and in some applications latter have more advantages on the former. Both modulated and unmodulated CW radars have wide application areas. Historically, proximity (VT) fuse and the frequency modulated continuous wave (FMCW) altimeter are the two early important applications of CW radar principle. The CW proximity fuse was first employed in artillery projectiles during World War II and the first practical model of FMCW altimeter was developed by the Western Electronic Company in 1938 [1].

Most of the theoretical works on FMCW radar were published during the period from the 1940s to the 1960s [2]. In addition to VT fuse and radio altimetry, FMCW radars developed for many areas in civil industry. This is due to the following features:

- Ability to measure small and very small ranges to the target, minimal measured range being comparable to the transmitted wavelength

- Ability to measure simultaneously the target range and its relative speed

- Small error of range measurement, which with some processing methods is within hundredths of a percent

- Ability to measure small range changes, which is less than fractions of a percent of the wavelength

- Signal processing after mixing is performed in a range of frequencies, commensurable with the modulation frequency, i.e. in a frequency band from hundreds of hertz up to hundreds of kilohertz, this considerably simplifies the realization of the processing circuits

- Small weight and energy consumption due to absence of high circuit voltages

- Compactness, the dimensions of a radar using modern technology being determined by the dimensions of the microwave block

1.1 Examples for Usage of FMCW Radar

1.1.1 Radio Altimeter

Radar altimeter is one of the early applications of FMCW radar that measures the altitude above the terrain and being used for airplanes or spacecrafts. It provides the distance between the plane and the ground. This type is used especially for landing in low visibility conditions. It is also very critical in low altitude flies and used as terrain avoidance system.

1.1.2 Proximity Fuse

A proximity fuse is designed to detonate an explosive automatically when the distance to target becomes smaller than a predetermined value. The proximity fuse was invented in the United Kingdom but developed mainly by the U.S. (with British collaboration) during World War II.

1.1.3 Level Measuring Radar

Level measuring radars are used most frequently used in liquid tanks. The transceiver antenna is placed on the cover of the tank. Antenna beam width is not very large and pointed vertically toward the surface of liquid. It measures range R from top to the liquid and liquid level L is obtained subtracting the R from the height H of the tank, i.e. $L = H\text{-}R$.

1.1.4 Naval Navigational Radar

FMCW radars can be applied to navigational radars with ranges up to several kilometers but FMCW radar is most useful at short ranges from tens to hundreds of meters that can be used for surveillance of the sea or large river ports when vessels arrive under conditions of bad visibility. FMCW radar can be used not only to search the water surface of the port but also to measure range and relative speed of any targets within the port [3].

1.1.5 Vehicle Collision Avoidance Radar

Vehicle collision warning systems have been developed in response to the substantial traffic growth in cities. This system usually includes four radar located at front, tail and two side mirrors. The front radar is critical, it provides continuous range and relative speed for targets and if necessary, a danger signal generated which can activate the brake system.

1.1.6 Precision Range Meter for Fixed Targets

For precision range measurement multi frequency CW radars using the phase processing of the reflected signals are being used. But to measure range of a fixed

target with multi frequency CW radar we must install an active reflector to simulate Doppler shift. On the other hand, FMCW radar is free from such a disadvantage and can be applied to such application.

1.1.7 Measurement of Very Small Motions

A typical example of small motion measurement is the observation of vibrations of various components of machines. For such measurement, a device, which has no physical contact with the vibrating component, is needed. FMCW radar simply solves problem for this application.

1.1.8 Hidden Object Detection

Examples of this type of application are the detection of voids in walls, the testing of homogeneity of building materials and the verification of the presence of reinforcing bars in concrete. In such applications, the depth of penetration is less of a problem, the main requirement being high resolution. In these cases, FMCW radar has considerable benefits over pulse radars [4].

There are of course other specific application areas of FMCW radars but these are the most popular application areas and enough to show that FMCW radar has wide application area.

1.2 Basic Short Range FMCW Radar Principle

The basic idea in a pulsed radar system to measure the range is the measurement of the time difference between the transmitted and the received signals. To do this in FMCW radar we should use a feasible idea, i.e. a timing mark, because we continuously transmit signal in continuous wave radar.

Modulation of some type is needed indeed to extract the range information from the signals. Amplitude, frequency or phase modulations are the choices. Amplitude modulation cannot be used in continuous wave radars because it is

practically impossible to distinguish the reflected signal from the interference caused by the background. Although amplitude modulation is not a solution for continuous wave, by means of frequency modulation time difference between the transmitted and received signals can be determined. By frequency modulating the carrier, FMCW radar is obtained in which the timing mark is the changing frequency. Transit time for transmitted and received signal is proportional to the frequency difference between two signals. When we have transmitted and received signals, operation of finding the time difference between the signals easily carried out by multiplication of the received signal and the transmitted signal. After multiplication a signal with frequency equal to the sum of the frequencies of the multiplied signals and a signal with frequency equal to the difference of the frequencies of the multiplied signals are formed. Former signal is to be eliminated by filtering out and the latter gives us the frequency difference and hence the range information of the target.

This thesis is mainly about the non-ideal behaviors in FMCW radars and range resolution improvement in a short-range FMCW radar system. There are different methods to improve range resolution in FMCW radar, which are mainly signal processing methods for the beat frequency, i.e. the frequency difference between the transmitted and the received signals. Improvement of range resolution is directly related to resolution of the beat frequency. In this study, improvement factors for the range resolution will be explained and a short-range FMCW radar range resolution improvement method will be proposed. In Chapter 2, basic FMCW radar principles and properties are explained. In addition, different aspects of the FMCW radar system, the non-ideal behaviors in the system are investigated and studies about reducing the effects of these behaviors done before this one mentioned. Chapter 3 gives derivations related with intermediate frequency (IF) signal processing method called spectral binning and brief definitions and comparison of some other methods for FMCW radar system. These methods are Fast Fourier Transform (FFT) and a model based on Auto

Regressive Moving Average (ARMA). In Chapter 4, range resolution improvement methods for alternative signal processing methods for FMCW radar are given. In Chapter 5, our prototype FMCW radar system components and properties of the system used in measurement setup are explained. A simple signal processing unit for short range FMCW radars is explained and measurement results for the prototype system is given.

CHAPTER 2

FREQUENCY MODULATED CONTINUOUS WAVE RADAR

In frequency modulated continuous wave (FMCW) radar, the transmitter frequency is varied as a function of time in a known manner. Assume that transmitter frequency increases linearly with time as shown in Fig. 2.1a. If there is a target at range R, an echo signal will return as shown in Fig. 2.1b. Time difference between the transmitted and the received signals is $T = 2R/c$.

(a)   (b)
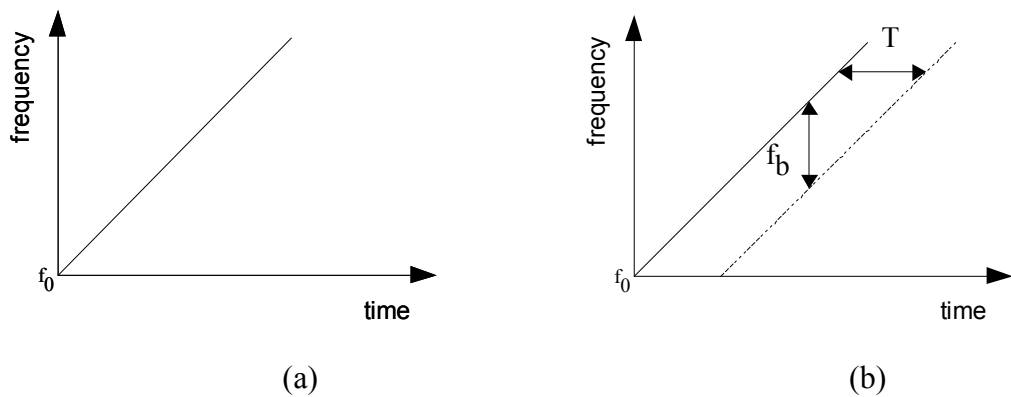
Fig. 2.1 Frequency change of (a) transmitted signal (b) transmitted and received signals

If the transmitted and the received signals are multiplied within a mixer then filtering out the high frequency term of the output we will get a beat

frequency f_b. When there is no Doppler shift in the signal, the beat frequency is a measure of the target's range and $f_b = f_r$ where f_r is the beat frequency due only to the target's range. If the slope of the frequency change of the transmitted signal is m_f then:

$$f_b = T \cdot m_f = \frac{2R}{c} \cdot m_f$$

(2.1)

In any practical CW radar, the frequency cannot be continuously changed in one direction only periodicity in the modulation is necessary. The modulation can be triangular, saw tooth, sinusoidal, etc. When triangular frequency modulated waveform is used as in Fig. 2.2 the resulting beat frequency will be as in Fig. 2.3.
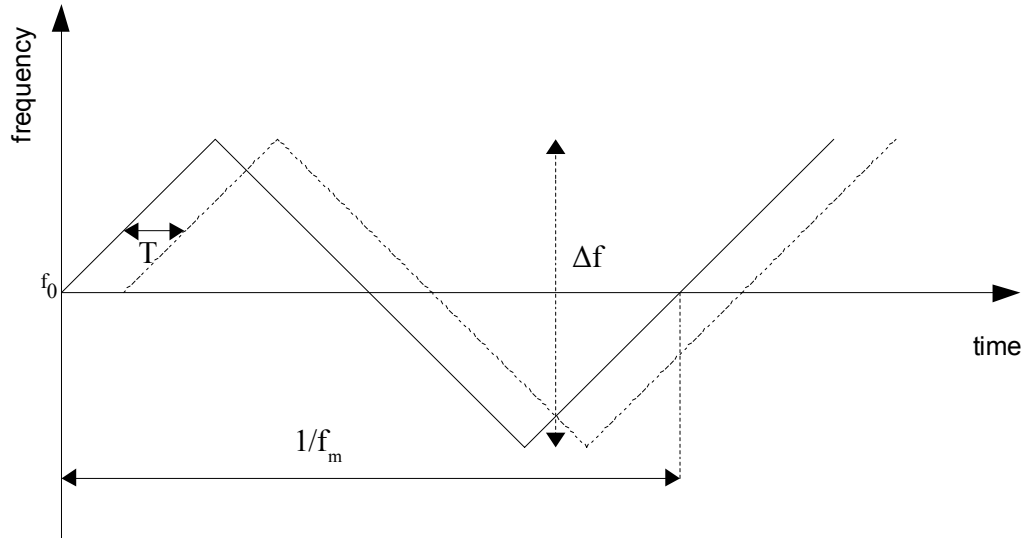
Fig. 2.2 Triangular frequency modulation for transmitted and received signals

8
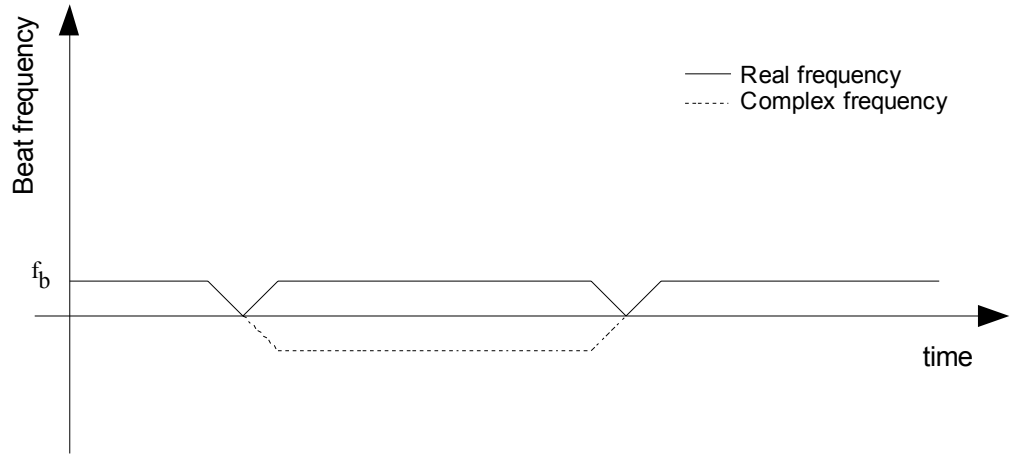
Fig. 2.3 The beat frequency of triangular frequency modulated signal

As shown in the Fig. 2.3, beat frequency is constant except at the turn-around region. If the frequency is modulated at a rate f_m and deviation of frequency is Δf then the beat frequency except the turn – around region is:

$$m_f = \frac{\Delta f}{1/2 f_m} = 2 f_m \Delta f \qquad (2.2)$$

Using (2.2) with (2.1):

$$f_b = \frac{4 R f_m \Delta f}{c} \qquad (2.3)$$

Thus as seen in (2.3) the measurement of the beat frequency determines the range R. If we define K factor as:

$$K = \frac{4 f_m \Delta f}{c} \qquad (2.4)$$

then

$$f_b = KR \qquad (2.5)$$

We can use two basic block diagrams to illustrate the principle of the FMCW radar. One is the structure with separate transmitting and receiving antennas as shown in Fig. 2.4 and the other structure is with only one antenna, which transmits and receives the signal as shown in Fig. 2.5. In either structure, a portion of transmitted signal acts as the reference signal to produce the beat frequency. This reference signal is introduced directly into the mixer. The isolation between transmitting and receiving antennas is critical to reduce transmitter leakage signal to a negligible level that arrives at the receiver via the coupling between antennas.
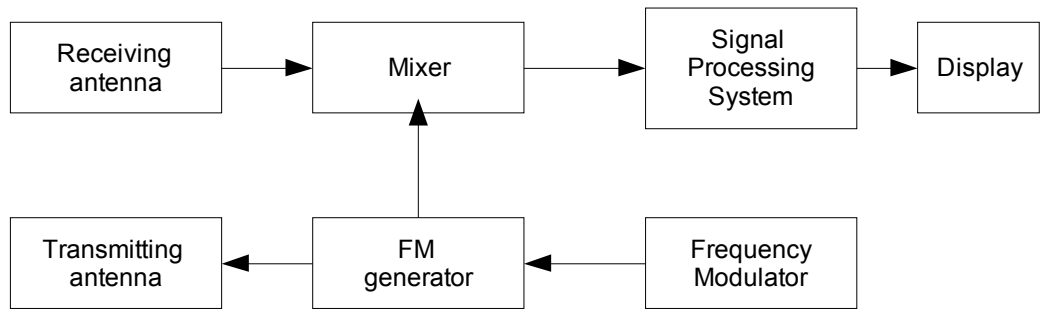
Fig. 2.4 Basic block diagram of an FMCW radar system with two antennas
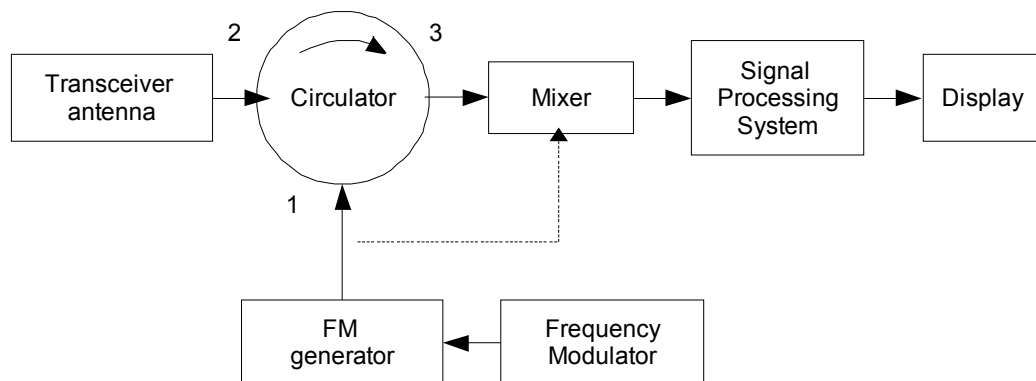
Fig. 2.5 Basic block diagram of an FMCW radar system with one antenna

In both structures the main idea is multiplication of the direct signal, i.e. a portion of transmitted signal which is fed to mixer, with the received signal, i.e. the echo signal reflected back from the target. The output of the mixer is called intermediate frequency (IF) signal, also called converted or distance measuring signal. IF signal is processed by some sort of processing system and information acquired is shown on the display. In Chapter 4, alternatives for signal processing part are explained.

The situation described in Fig. 2.2 and Fig. 2.3 is the case when the target is stationary. If the target is moving, there will be a Doppler frequency shift superimposed to the beat frequency and it should be considered in the demodulation. The Doppler frequency shifts the frequency – time plot of the echo (received) signal according to relative direction of the target's velocity. The frequency – time plot of the transmitted and the echo signals for moving target is given in Fig. 2.6.
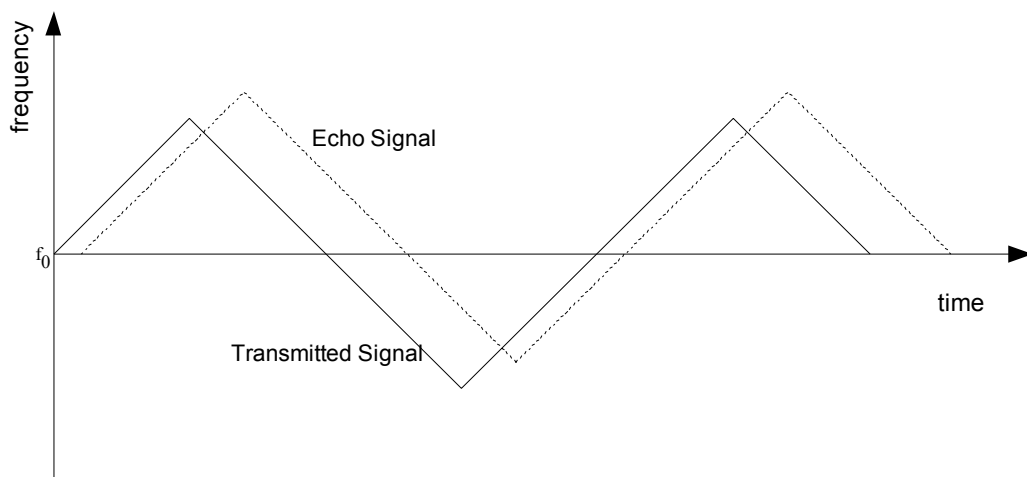
Fig. 2.6 Frequency of the transmitted and the echo signals with Doppler shift
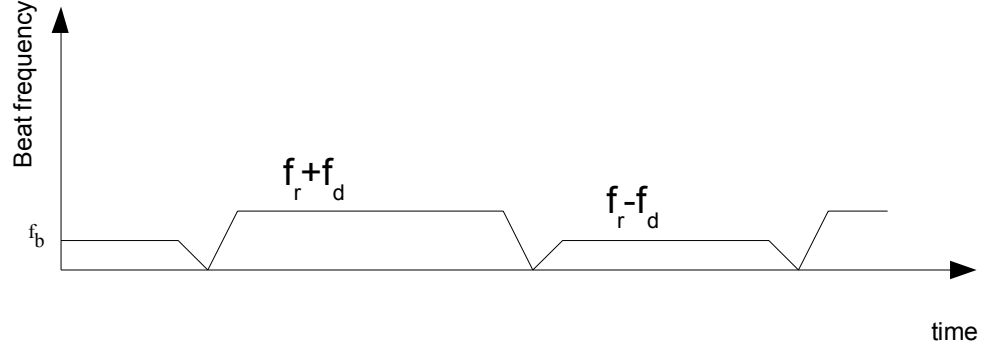
Fig. 2.7 The beat frequency with Doppler shift

As shown in Fig. 2.7 on one portion of the frequency modulation cycle, the beat frequency is increased by the Doppler shift, while on the other portion it is decreased by the same amount. Therefore the beat frequency is switched between $f_{b1} = f_r + f_d$ and $f_{b2} = f_r - f_d$. For this situation switching the frequency counter every half cycle and measuring the beat frequency separately as f_{b1} and f_{b2} is needed. The beat frequency directly related to target range, f_r, is extracted by averaging the two beat frequencies that is $f_r = (f_{b1} + f_{b2})/2$ also the Doppler frequency can be extracted by subtracting two beat frequencies that is $f_d = (f_{b1} - f_{b2})/2$.

As can be seen in (2.5) processing the IF signal for both Doppler shift and without Doppler shift case, range information is obtained easily. Some of the methods for IF signal processing is addressed in chapter 4. There are some non-ideal behaviors in the FMCW system and most important ones can be addressed as:

- Transmitter Leakage

12

- Nonlinear Frequency Sweep
- Measurement Errors

2.1 Transmitter Leakage

One of the most important factors that must be addressed is leakage of the transmitter signal into the receiver. The problems associated with this leakage are not insuperable but they must be treated carefully for a successful FMCW system implementation. Any CW radar must be able to receive at the same time as it is transmitting. This means that the inevitable direct breakthrough of the transmitter signal into the receiver must be controlled to stop it degrading the receiver sensitivity. The most severe problem occurs when the leakage signal is so powerful that it threatens to saturate the receiver mixer. Even at lower power levels, the noise sidebands on the transmitted signal may still degrade the receiver sensitivity if care is not taken. For low power radars, actual damage of the receiver is not normally the problem.

The leakage is mainly due to the leakage to the isolated terminal of the circulator and reflections from antenna. Therefore, these problems include a limit to the maximum transmitted power, a requirement for careful matching of the antenna to reduce the reflections from antenna and a highly isolated circulator to minimize the magnitude of the reflections and leakage back into the receiver. For a typical single antenna structure with circulator, isolation between the transmitter and the receiver is about 15 – 20 dB, which can be improved by careful design to about 30 – 35 dB over a narrow frequency band [3].

2.1.1 Separate Transmit and Receive Antenna

The simplest way of achieving greater isolation is to use separate antennas for transmission and reception. Although this improves the isolation drastically, the effects of noise leakage cannot necessarily be ignored. In addition, advantage of using only one antenna is lost.

2.1.2 Reflected Power Canceller

When the use of two antenna is not desired, the level of the transmit/receive leakage can be reduced by using a simple leakage canceller which subtracts the amount of the leakage signal from the signal fed to the mixer. The canceller signal can be determined for the system without the target, i.e. only the leakage signal is measured, and this signal level is used as canceller signal level. This simple idea can be improved to an adjustable canceller as in Fig. 2.8.
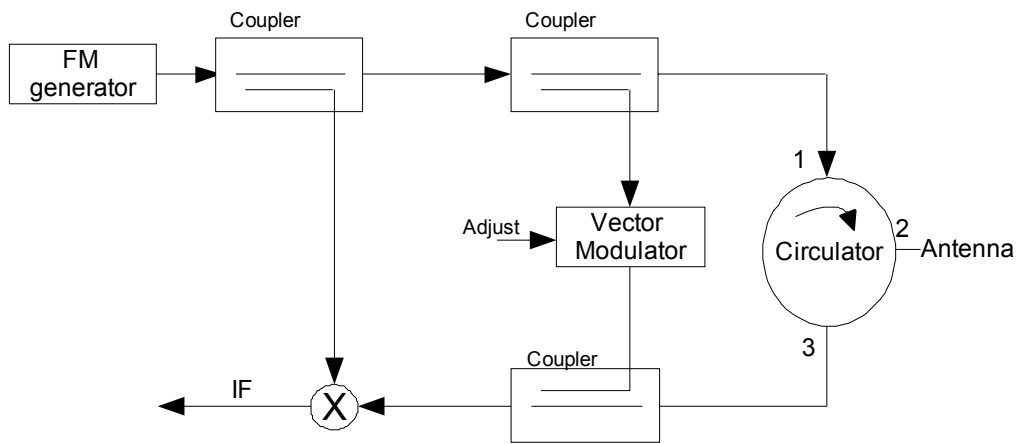
Fig. 2.8 Adjustable leakage power canceller

In the configuration of Fig. 2.8 a small fraction of the transmitted power is coupled and fed into a vector modulator, i.e. phase shifter plus attenuator, to produce the cancellation signal whose amplitude and phase can be adjusted to match the combined leakage and reflected power from antenna exactly. By adding this signal into the receiver via a coupler, the leakage including the noise sidebands of the transmitted signal can be cancelled out. Such cancellers appreciated for a long time and practical implementations have been investigated since 1960s. The effectiveness of this method depends upon the accuracy with

which the amplitude and phase can be adjusted. In a practical system, this canceller must be a closed loop with sufficient gain and bandwidth to track the leakage variations. A possible solution is a reflected power canceller (RPC) of Fig. 2.9.
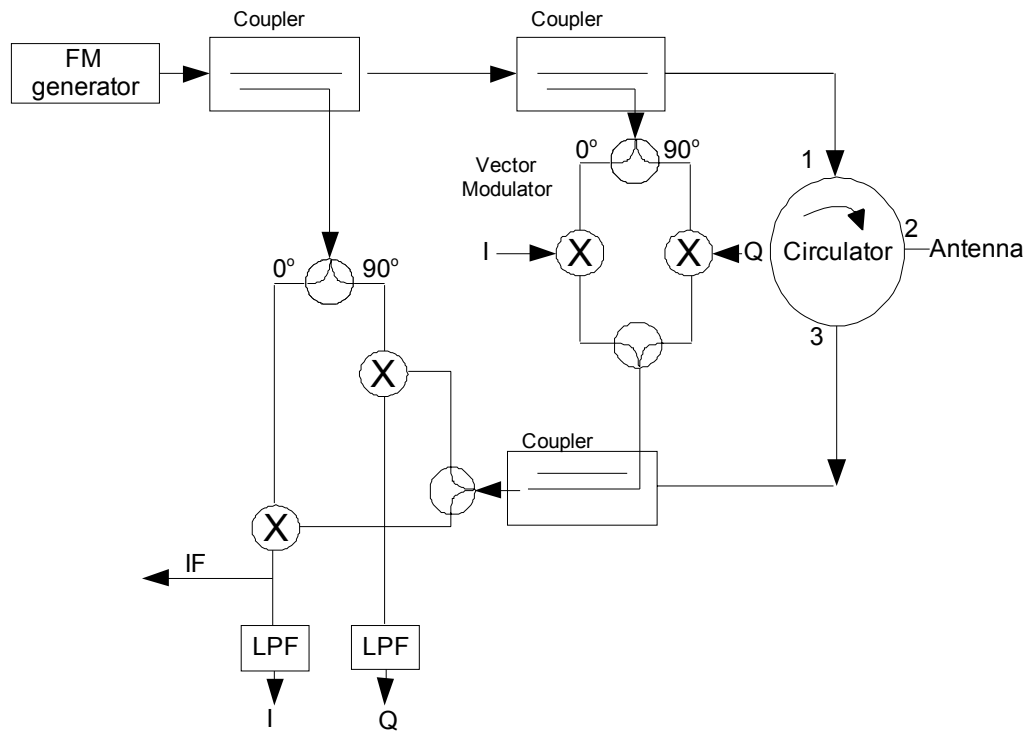
Fig. 2.9 Adaptive reflected power canceller

The basic principle of the adaptive RPC is shown in Fig. 2.9. The amplitude and phase of the leakage power are estimated by measuring the DC levels of the inphase (I) and quadrature (Q) outputs of the receiver mixer. These I and Q signals then used to control the amplitude and phase of the canceller signal. The RPC forms a closed loop controller.

The control loops for the I and Q channels are essentially independent, which means that leakage of signals from one channel to the other, due to the lack of ideality in the components, merely acts as disturbance in the other channel. With a reasonable level of loop gain, this disturbance has only a small effect on the overall performance of the loop, so the RPC is quite robust to phase errors of the order of 45 degrees around the loop, which means that the specifications of the vector modulator and of the quadrature mixer do not need to be particularly stringent.

The idea has been revived for the PILOT navigation radar, using modern microwave component techniques and a simplified phase compensation scheme. In the PILOT case, the RPC improves the transmit/receive isolation from about 20 dB to about 50 dB, which is comparable with the isolation obtained from a dual antenna system [6].

2.2 Nonlinear Frequency Sweep

The range resolution is dependent on the chirp linearity. As shown conceptually in Fig. 2.11 if the chirp is not linear, then the beat frequency for a point target will not be constant and the range resolution will suffer.
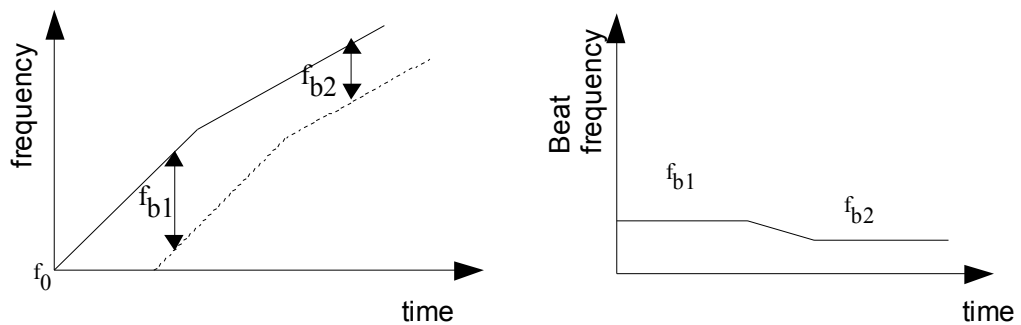
Fig. 2.10 Effect of the Chirp Nonlinearity on the Beat Frequency

16

This limitation is one of the fundamental problems with the FMCW radar system and has been addressed in a number of ways that are discussed later in this work. If the nonlinear case is considered the chirp bandwidth is increased the range resolution will improve, but simultaneously the total nonlinearity increases and the range resolution degrades. In addition, the time variant beat frequency results in smeared frequency spectrum.

The nonlinear frequency dependence of the voltage controlled oscillator (VCO) and the combined non-flat in-band response of all the components in the system results in the nonlinearities in signal frequency. There are several techniques for linearization of the VCO frequency sweep, which is the crucial nonlinearity source of the system. The techniques are mainly hardware based but there are also some reported software based solutions [7], [8]. The hardware based solutions are mainly of two types: first one is the open loop correction, which modifies the VCO tuning voltage properly to get a linear chirp, i.e. voltage predistortion, and the second one is the closed loop, which adopts a phase locked loop circuitry.

2.2.1 Open Loop Correction

Frequency of the VCO can be changed by varying the voltage at its control input. This voltage at the control input is called the tuning voltage and its relationship with the frequency gives the tuning curve of the VCO. Generally, without any correction, the voltage and frequency response of the VCO do not have a linear relationship. In order to obtain a linear frequency sweep output, a nonlinear voltage ramp is applied at the input. The common method uses the programmed correction stored in a lookup table, which is then clocked through a digital to analog converter (DAC). The VCO temperature must either be held constant or different lookup tables must be used to accommodate variations in the oscillator characteristic [9], [10].
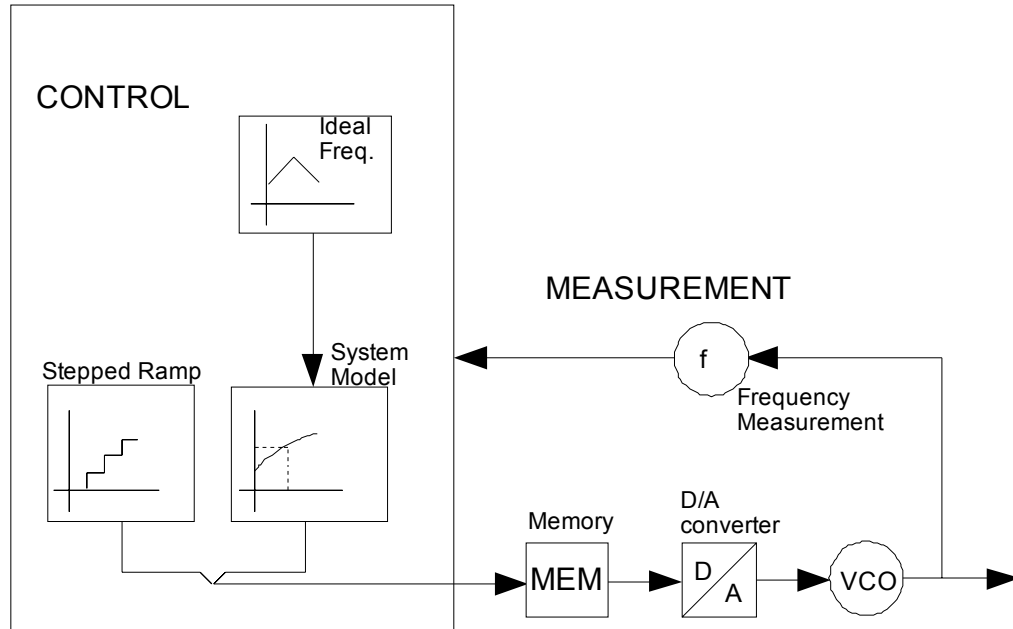
Fig 2.11 Simplified block diagram for open loop correction

Fig. 2.11 shows a typical open loop correction application, using voltage predistortion. The dependency of frequency onto voltage is to be measured by applying a sequence of constant tuning voltages, which is increased by a small amount between successive measurements, to the VCO tuning input and measuring the respective output frequency. Given a sampled version of the ideal frequency curve, the corresponding voltage sequence that has to be applied to the VCO tuning input can be found by interpolation. A source of error of this approach is any difference between the frequency measurement in the static case, i.e. with constant input voltage, and the final output frequency during ramp generation. In addition, as mentioned before since the frequency is controlled only by an open-loop system, inevitable frequency drifts due to temperature, environmental conditions, aging, etc. cannot be compensated for.

2.2.2 Closed Loop Correction

Incorporating the VCO into a feedback loop to stabilize its oscillation frequency lead to the concept of phase-locked loops (PLLs) that lock the RF output frequency to the phase of a stable reference oscillator. Building blocks of a typical PLL are shown in Fig. 2.12. The phase-frequency detector (PFD) converts phase differences between its input signals to short current impulses of proportional duration. A loop filter averages these pulses and implements the loop control function. The RF signal generated by the VCO is output for FMCW sensing, and is also fed back to the PFD via a variable frequency divider that can be used to introduce phase or frequency modulation.

As PLLs are dynamic systems, any changes in the system input will cause the output not to follow immediately, but to exhibit some transient behavior. Such errors in the output frequency will have a negative influence on the FMCW measurement result, if the deviation decays slowly compared to the total ramp duration. For fast frequency ramps typical transients may take up to the total ramp time, leading to frequency ramps unusable for FMCW distance sensing.

A novel method that allows the measurement of the instantaneous VCO output phase within the PLL without the use of external measurement equipment can be used [11]. Knowledge of the frequency error with respect to the ideal curve can then be used to compute a suitable adaptation of the divider input sequence.
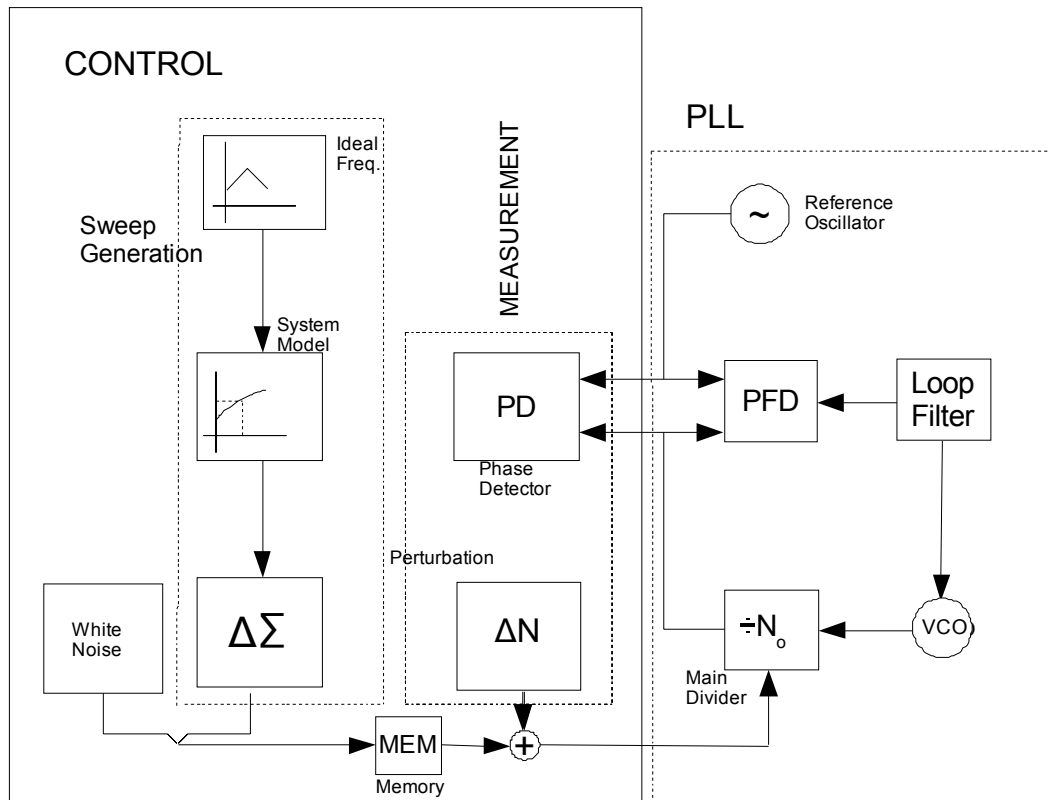
Fig 2.12 Block diagram for closed loop correction method

The method allows the approximate measurement of the VCO output frequency at the time instants of rising edges of the reference signal. It requires the addition of a second phase detector to the standard phase-locked loop as sketched in Fig. 2.12 that allows determination of the leading edge of the two PFD input signals in every reference oscillator cycle. The VCO output frequency produced by a periodic divider value input sequence can then be determined by applying appropriate modifications to the unperturbed input sequence, while observing the influence of this modification on the succession of the PFD input signal edges.

Being able to obtain a phase estimate to a known input sequence, a linear model of the PLL may easily be computed. From a measurement of the phase deviation

for a periodic input sequence with respect to the ideal curve, the required predistortion of the input divider sequence can be computed using the obtained dynamic system model. Since the main divider only allows integer valued input, Delta-Sigma modulation has to be performed on the theoretical divider sequence. Due to measurement inaccuracy and model approximations a single-step compensation will cause residual phase error, which can however be minimized by iterative application of the adjustment procedure.

2.3 Measurement Errors

The accuracy of the radar is usually of more importance at short ranges than the long ranges. Errors of a few meters might not be of significance for long ranges but are important for short-range measurements. The theoretical accuracy with which distance can be measured depends on the bandwidth of the transmitted signal and the ratio of signal energy to noise energy (SNR). In addition, measurement accuracy might be limited by such practical restrictions as the accuracy of the frequency-measuring device, linear frequency sweep nonlinearities, errors caused by multiple reflections and transmitter leakage, the residual path length error caused by circuits and transmission lines and the frequency error due to the turn around regions of the frequency modulation.

If cycle counter, which measures the number of cycles or half cycles of the beat during the modulation period, is used as a frequency-measuring device then the total cycle count is a discrete number since the counter is unable to measure fractions of a cycle. The discreteness of the frequency measurement gives rise to an error called the fixed error, or quantization error. The average number of cycles N of the beat frequency f_b in one period of the modulation cycle f_m is $\overline{f_b}/f_m$ where the bar over f_b denotes time average. (2.3) may be written as:

$$R = \frac{cN}{4\Delta f} \qquad (2.6)$$

Since output of the frequency counter N is an integer, the range will be an integral multiple of

$c/4\Delta f$ and will give rise to quantization error equal to:

$$\delta R = \frac{c}{4\Delta f} \qquad\qquad (2.7)$$

Note that the fixed error is independent of the range and carrier frequency and is a function of frequency excursion only. Large frequency excursions are necessary if the fixed error is to be small.

Besides these non-ideal properties the FM to AM distortion is another important effect that is a combined effect of all the individual modules. All the modules have frequency dependent transfer characteristics which result in a AM distortion in the signal.

As given in Chapter 5, a prototype FMCW radar is constructed and measurements are carried. The components in the prototype are not ideal, and special precautions are not taken to compensate the non-ideal properties. That is, the nonlinear frequency sweep and FM to AM distortion are present in the prototype. Because of this reason, the measured spectra do not exactly match with the expected ideal behavior.

The leakage from the transmitter to receiver is prevented by using two different antennas (terminals) for measurement as explained in Chapter 5.

These non-ideal properties are limitations for all implementations. The analyses in the following sections are carried out by discarding these properties, but the prototype unavoidably suffers from these effects. Therefore, the proposed method is demonstrated to be able to operate in non-ideal situations.

CHAPTER 3

SIGNAL PROCESSING FOR FMCW

FMCW radars operate using the homodyne principle, i.e. CW radar in which the oscillator serves as both the transmitter and the local oscillator. As can be seen in Fig. 3.1 the signal is frequency modulated to produce a linear chirp which is radiated toward a target through an antenna. The echo received T_d seconds later, which is shown in Fig. 3.2, is mixed with a portion of transmitted signal to produce a beat signal at frequency f_b, which is directly proportional to round trip time T_d as can be seen in (1.3)
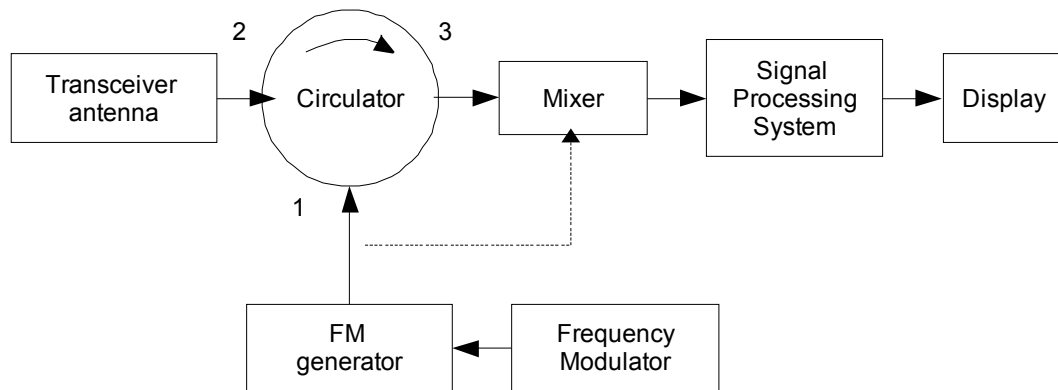
Fig. 3.1 Basic block diagram of an FMCW radar system with one antenna
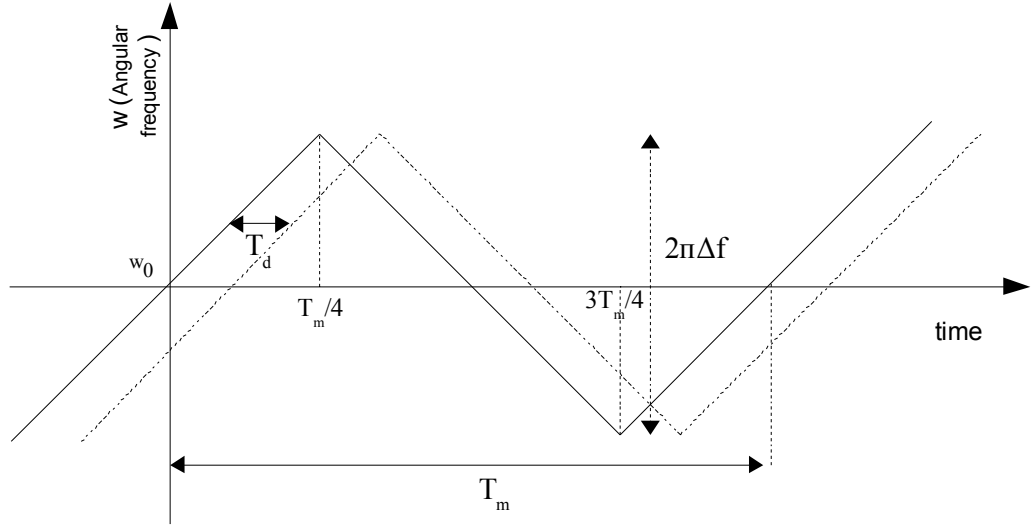
Fig. 3.2 The frequency of the transmitted and the received signal waveforms

3.1 Determining Beat Frequency

The change in the frequency ω_b with time can be described by the following two equations, for positive and negative slope regions:

$$\omega^+ = \omega_o + mt \tag{3.1}$$

$$\omega^- = \omega_o - mt \tag{3.2}$$

where slope m is:

$$m = \frac{2\pi\Delta f}{T_m / 2} = 4\pi\Delta f \cdot f_m \tag{3.3}$$

The transmitted frequency modulated signal is

$$v_t(t) = A_t \cos(\Phi(t)) \tag{3.4}$$

where

$$\omega^+ = \frac{d\Phi^+(t)}{dt} = \omega_o + mt \tag{3.5}$$

24

integrating (3.5) we get

$$\Phi^{+}\left(t\right)=\omega_{o}t+\frac{1}{2}mt^{2}+\Phi_{o} \tag{3.6}$$

substituting (3.6) into (3.4) we get

$$v^{+}_{t}\left(t\right)=A_{t}\cos\left(\omega_{o}t+\frac{1}{2}mt^{2}+\Phi_{o}\right) \tag{3.7}$$

The echo signal is the time-delayed version of the transmitted signal with different amplitude A_r and different phase Φ_1 :

$$v^{+}_{r}\left(t\right)=A_{r}\cos\left(\omega_{o}\left(t-T_{d}\right)+\frac{1}{2}m\left(t-T_{d}\right)^{2}+\Phi_{1}\right) \tag{3.8}$$

The mixer output signal, i.e. IF signal, will be product of these two signals:

$$v^{+}_{out}\left(t\right)=v_{t}^{+}\left(t\right)\times v_{r}^{+}\left(t\right) \tag{3.9}$$

Using the known trigonometric relations, we can expand the product of (3.7) and (3.8):

$$v^{+}_{out}\left(t\right)=\frac{1}{2}A_{t}A_{r}\left[\begin{array}{l}\cos\left(\left(2\omega_{o}-mT_{d}\right)t+mt^{2}+\Phi_{m1}\right)\\ +\cos\left(mT_{d}t+\Phi_{m2}\right)\end{array}\right] \tag{3.10}$$

defining $\Phi_{m1}=\frac{1}{2}mT_{d}-\omega_{o}T_{d}^{2}+\Phi_{o}+\Phi_{1}$, $\Phi_{m2}=\omega_{o}T_{d}-\frac{1}{2}mT_{d}^{2}+\Phi_{o}-\Phi_{1}$.

The first cosine term describes a linearly increasing FM signal (chirp) at about twice the carrier frequency with a phase shift that is proportional to the delay time Td. This term generally filtered out actively by low pass filter (LPF) after mixer. The second cosine term describes the beat signal at a fixed frequency, which can be obtained by differentiating the instantaneous phase term with respect to time. Fig. 3.3 shows the output signal spectrum prior to filtering that contains both the linear chirp and the constant frequency components [5].

25
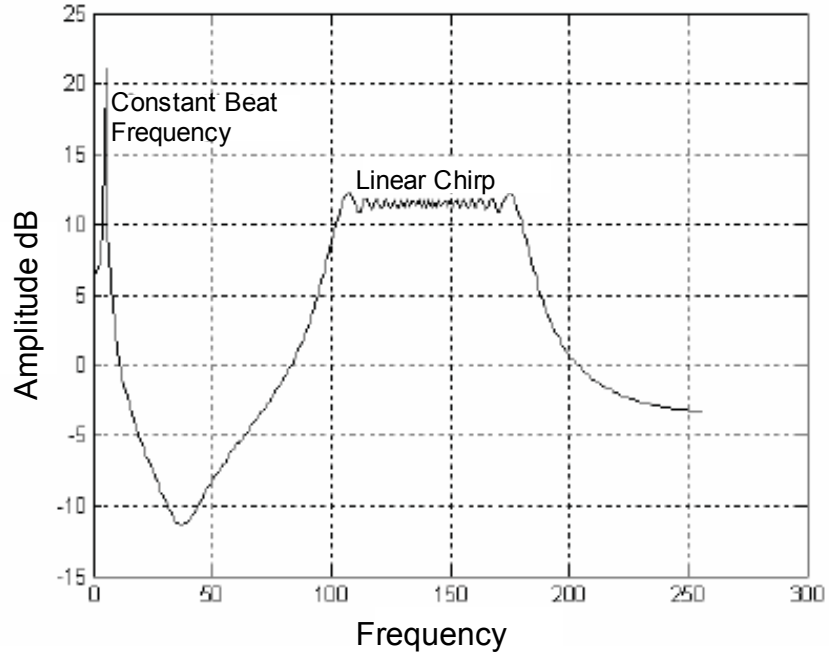
Fig. 3.3 FMCW radar mixer output spectrum

To obtain beat frequency, use phase of the second term:

$$f_b = \frac{1}{2\pi} \frac{d}{dt} \left[mT_d t + \omega_o T_d - \frac{1}{2} mT_d^2 + \Phi_o - \Phi_1 \right]$$ (3.11)

Using (3.3) and (3.11) with $T_d = 2R/c$:

$$f_b = \frac{4\Delta f \cdot f_m R}{c}$$ (3.12)

It can be seen that the beat frequency is directly proportional to the range of the target. Therefore, by determining the beat frequency the range can be determined directly.

3.2 Analysis of the Beat Frequency Signal for Spectral Binning

To inspect Fourier transform of the beat signal in Fig. 3.2, the signal can be analyzed for positive slope regions and for the negative slope regions separately. After finding the Fourier series coefficients for both parts, Fourier transform of the signal can be easily found. Calling the time independent phase term in the filtered mixer output signal as of (3.10) as Φ^+_a

$$\Phi^+_a = \omega_o T_d - \frac{1}{2}mT_d^2 + \Phi_o - \Phi_1 \qquad (3.13)$$

Then the filtered mixer output signal for the positive slope region can be rewritten from (3.10) as follows:

$$v^+_{out}(t) = \cos\left(mT_d t + \Phi^+_a\right) \qquad (3.14)$$

This signal can be written in terms of Fourier series expansion as follows:

$$F^+(t) = V^+_{out}(t) = \sum_{n=-\infty}^{n=\infty} \frac{C_n^+}{T_m} e^{j\omega_n t} \qquad (3.15)$$

where $V^+_{out} = e^{j\Phi^+_a}e^{j\omega_b t}$.

$$C_n^+ = \int_{-\frac{T_m}{2}}^{\frac{T_m}{2}} V^+_{out} e^{-j\omega_n t} dt \qquad (3.16)$$

where $\omega_n = n\omega_m = \dfrac{2\pi n}{T_m} = 2\pi n f_m$ and

$$\omega_b = 2\pi f_b = mT_d \qquad (3.17)$$

If we write (3.14) using phasor V^+_{out}

$$v^+_{out}(t) = \text{Re}\left\{V^+_{out}\right\} \qquad (3.18)$$

27

Using phasor expression in (3.16) and changing the integration limits according to the region where C_n^+ is non-zero:

$$C_n^+ = \int_{-\frac{T_m}{4}+T_d}^{\frac{T_m}{4}} e^{j\Phi^+_a} e^{j\omega_b t} e^{-j\omega_n t} dt \tag{3.19}$$

$$C_n^+ = \frac{e^{j\Phi^+_a}}{j\Omega_n} \left(e^{j\Omega_n \frac{T_m}{4}} - e^{-j\Omega_n \frac{T_m}{4}} . e^{j\Omega_n T_d} \right) \tag{3.20}$$

where $\Omega_n = \omega_b - \omega_n$.

This is the expression for Fourier series coefficients of filtered mixer output signals for positive slope region. Negative slope region considered separately, the derivation is similar to the positive slope regions. It will be considered that negative slope parts shifted to the origin as in Fig. 3.4.
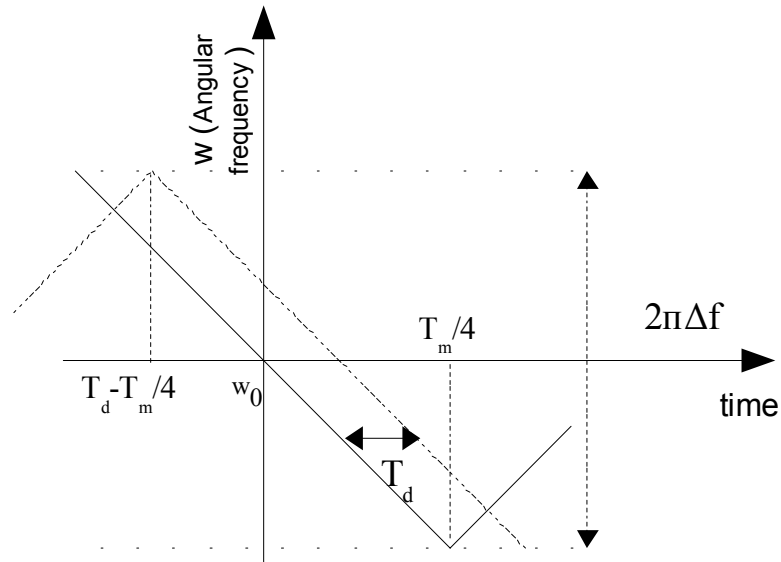
Fig. 3.4 Negative slope parts shifted to origin

Call shifted version of negative slope part as F^- :

$$F^-(t) = v^-{}_t\left(t - \frac{T_m}{2}\right) \tag{3.21}$$

If we do the same calculations done in $(3.4) - (3.9)$ with only one difference that is replace ω^- with ω^+ of (3.1) as follows:

$$\omega^- = \frac{d\Phi^-(t)}{dt} = \omega_o - mt \tag{3.22}$$

integrating (3.22)

$$\Phi^-(t) = \omega_o t - \frac{1}{2}mt^2 - \Phi_o \tag{3.23}$$

Substituting (3.23) into (3.4) for negative slope parts we get

$$v^-{}_t(t) = A_t \cos\left(\omega_o t - \frac{1}{2}mt^2 - \Phi_o\right) \tag{3.24}$$

The echo signal is the time-delayed version of the transmitted signal:

$$v^-{}_r(t) = A_r \cos\left(\omega_o\left(t - T_d\right) - \frac{1}{2}m\left(t - T_d\right)^2 - \Phi_1\right) \tag{3.25}$$

For (3.24) and (3.25), after following the steps which are similar to those followed for (3.9) and (3.10) we get the filtered mixer output signal for the negative slope region from equation as:

$$v^-{}_{out}(t) = \cos\left(\omega_b t + \Phi^-{}_a\right) \tag{3.26}$$

where

$$\Phi^-{}_a = \Phi_o - \Phi_1 - \omega_o T_d - \frac{1}{2}mT_d^2 \tag{3.27}$$

$v^-{}_{out}(t)$ can be written in terms of Fourier series coefficients C_n as follows:

$$v^-_{out}(t) = \sum_{n=-\infty}^{n=\infty} \frac{C_n^-}{T_m} e^{j\omega_n t} \tag{3.28}$$

where

$$C_n^- = \int_{-\frac{T_m}{2}}^{\frac{T_m}{2}} V^-_{out}(t) e^{-jw_n t} dt \tag{3.29}$$

and $V^-_{out} = e^{j\Phi^-_a} e^{j\omega_b t}$.

Changing the integration limits of (3.29) according to the region where C_n^- is non-zero:

$$C_n^- = \int_{-\frac{T_m}{4}+T_d}^{\frac{T_m}{4}} e^{j\Phi^-_a} e^{j\omega_b t} e^{-j\omega_n t} dt \tag{3.30}$$

$$C_n^- = \frac{e^{j\Phi^-_a}}{j\Omega_n} \left(e^{j\Omega_n \frac{T_m}{4}} - e^{-j\Omega_n \frac{T_m}{4}} \cdot e^{j\Omega_n T_d} \right) \tag{3.31}$$

Now we can find Fourier transformation of filtered mixer output signal as follows

$$\tilde{F}(\omega) = \mathsf{F}\{F^+(t) + F^-(t)\} = \mathsf{F}\{F^+(t)\} + \mathsf{F}\{F^-(t)\} = \tilde{F}^+(\omega) + \tilde{F}^-(\omega) \tag{3.32}$$

From (3.15) we can easily write:

$$\tilde{F}^+(\omega) = \sum_{n=-\infty}^{n=\infty} \frac{C_n^+}{T_m} 2\pi\delta(\omega - \omega_n) \tag{3.33}$$

and of course (3.28) should change for F^- as follows

$$F^-(t) = v^-_{out}(t - \frac{T_m}{2}) = \sum_{n=-\infty}^{n=\infty} \frac{C_n^-}{T_m} e^{-j\omega_n \frac{T_m}{2}} \cdot e^{j\omega_n t} \tag{3.34}$$

Then from (3.34) we can write

$$\tilde{F}^-(\omega) = \sum_{n=-\infty}^{n=\infty} \frac{C_n^-}{T_m} e^{-j\omega_n \frac{T_m}{2}} 2\pi\delta(\omega - \omega_n) \qquad (3.35)$$

Recalling (3.32) to have a compact form:

$$\tilde{F}(\omega) = \tilde{F}^+(\omega) + \tilde{F}^-(\omega) \qquad (3.36)$$

and we need to write C_n^- in terms of C_n^+, use (3.20) and (3.31)

$$\frac{C_n^-}{C_n^+} = e^{-j(\Phi^+{}_a - \Phi^-{}_a)} = e^{-j2\omega_o T_d} \qquad (3.37)$$

where (3.13) and (3.27) used to obtain $\Phi^+{}_a - \Phi^-{}_a = 2\omega_o T_d$.

Substituting (3.33), (3.35) and (3.37) into (3.36)

$$\tilde{F}(\omega) = \sum_{n=-\infty}^{n=\infty} \frac{C_n^+}{T_m} \left[1 + e^{-j(2\omega_o T_d + \omega_n \frac{T_m}{2})} \right] 2\pi\delta(\omega - \omega_n) \qquad (3.38)$$

To reduce final equation we can call new coefficients C_n as follows and use

$$C_n = \frac{2\pi}{T_m} C_n^+ \left(1 + e^{-j\left(2\omega_o T_d + \omega_n \frac{T_m}{2}\right)} \right) \qquad (3.39)$$

$$C_n = \frac{2\pi}{T_m} C_n^+ e^{-j\left(\omega_o T_d + \omega_n \frac{T_m}{4}\right)} 2\cos\left(\omega_o T_d + \omega_n \frac{T_m}{4}\right) \qquad (3.40)$$

In order to obtain an explicit form for (3.40), (3.20) can be modified as follows:

$$C_n^+ = \frac{e^{j\Phi^+{}_a}}{j\Omega_n} e^{j\Omega_n \frac{T_d}{2}} \left(e^{j\Omega_n \frac{T_m}{4}} \cdot e^{-j\Omega_n \frac{T_d}{2}} - e^{-j\Omega_n \frac{T_m}{4}} \cdot e^{j\Omega_n \frac{T_d}{2}} \right) \qquad (3.41)$$

to simplify (3.41):

$$C_n^+ = \frac{e^{j\Phi^+{}_a}}{j\Omega_n} e^{j\Omega_n \frac{T_d}{2}} \cdot 2j \cdot \sin\left[\Omega_n\left(\frac{T_m}{4} - \frac{T_d}{2}\right)\right]$$

(3.42)

$$C_n^+ = e^{j\left(\Phi^+{}_a + \Omega_n \frac{T_d}{2}\right)}\left(\frac{T_m}{2} - T_d\right)\frac{\sin\left[\frac{\Omega_n}{2}\left(\frac{T_m}{2} - T_d\right)\right]}{\frac{\Omega_n}{2}\left(\frac{T_m}{2} - T_d\right)}$$

(3.43)

The magnitude of the Fourier series coefficients gives spectrum we need, substituting (3.43) into (3.40):

$$|C_n| = \frac{4\pi}{T_m} \cdot \left|\frac{T_m}{2} - T_d\right| \cdot \left|\cos\left(w_0 T_d + w_n \frac{T_m}{4}\right)\right| \cdot \left|\frac{\sin\left[\frac{\Omega_n}{2}\left(\frac{T_m}{2} - T_d\right)\right]}{\frac{\Omega_n}{2}\left(\frac{T_m}{2} - T_d\right)}\right|$$

(3.44)

(3.44) can be written in the form:

$$|C_n| = 2\pi\left|\left(1 - \frac{2T_d}{T_m}\right)\right| C_{dn}\overline{C}_n$$

(3.45)

where C_{dn} and $\overline{C}_n$ are:

$$|\overline{C}_n| = \left|\frac{\sin\left[\left(\omega_b - \omega_n\right)\left(\frac{T_m}{4} - \frac{T_d}{2}\right)\right]}{\left(\omega_b - \omega_n\right)\left(\frac{T_m}{4} - \frac{T_d}{2}\right)}\right|$$

(3.46)

$$C_{dn} = \left|\cos\left(\omega_o T_d + \omega_n \frac{T_m}{4}\right)\right|$$

(3.47)

for the nulls of the $\overline{C}_n$:

32

$$(\omega_b - \omega_n)\left(\frac{T_m}{4} - \frac{T_d}{2}\right) = \pm\pi \tag{3.48}$$

$$\omega_n = \omega_b \pm \frac{\pi}{\frac{T_m}{4} - \frac{T_d}{2}} = \omega_b \pm \frac{2\omega_m}{\left(1 - \frac{2T_d}{T_m}\right)} \tag{3.49}$$

Note that $\left(1 - \dfrac{2T_d}{T_m}\right) \approx 1$ under the assumption $T_m >> 2T_d$.

For C_{dn} use $\omega_n \dfrac{T_m}{4} = n\omega_m \dfrac{T_m}{4} = n\dfrac{\pi}{2}$ with (3.47):

$$C_{dn} = \left| \cos\left(\omega_o T_d\right) \cdot \cos\left(n\frac{\pi}{2}\right) - \sin\left(\omega_o T_d\right) \cdot \sin\left(n\frac{\pi}{2}\right) \right| \tag{3.50}$$

$$C_{dn} = \begin{cases} \left|\cos\left(\omega_o T_d\right)\right|, n = even \\ \left|\sin\left(\omega_o T_d\right)\right|, n = odd \end{cases} \tag{3.51}$$

The beat frequency carrier may be lost if n = even and $\omega_o T_d = \pi/2$ or n = odd and $\omega_o T_d = \pi$. Since very small changes in the range make enough change for $\omega_o T_d$ to prevent the occurrence of the beat frequency carrier annihilation, the probability of occurrence of the beat frequency annihilation is very small. (3.38) can be written in the following form where C_n defined in (3.39)

$$\tilde{F}(\omega) = \sum_{n=-\infty}^{n=\infty} C_n 2\pi\delta(\omega - \omega_n) \tag{3.52}$$
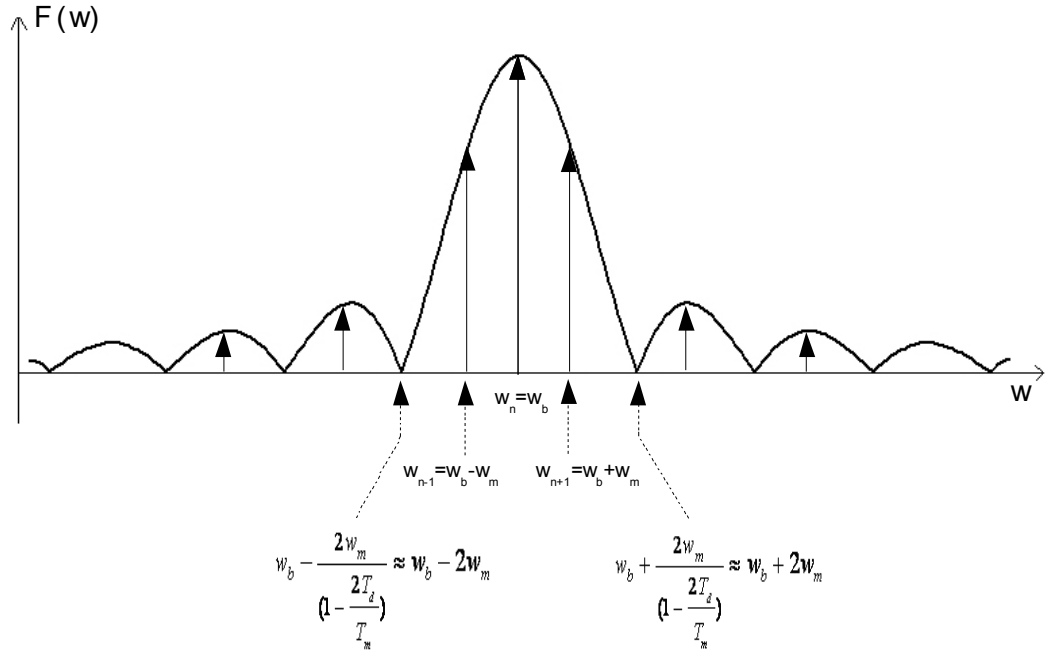
Fig. 3.5 Fourier transform of the IF signal

The ranges corresponding to the beat frequencies which are integer multiples of the modulation frequency ω_m give the maximum echo amplitude at the modulation harmonics. That is C_n of (3.44) maximizes at ω_n when $\omega_m = \omega_n = n\omega_m$. The range resolution corresponding to two adjacent harmonics ω_n and ω_{n+1} is ΔR. Using (3.12) for $\omega_{b1} = \omega_n$ and $\omega_{b2} = \omega_{n+1}$:

$$\omega_{b1} = \omega_n = \frac{4\Delta f . \omega_m R_1}{c} \tag{3.53}$$

$$\omega_{b2} = \omega_{n+1} = \frac{4\Delta f . \omega_m R_2}{c} \tag{3.54}$$

from (3.52) and (3.53):

34

$$\omega_{n+1} - \omega_n = \omega_m = \frac{4\Delta f . \omega_m}{c}\left(R_2 - R_1\right) \qquad (3.55)$$

Finally, we get range resolution as:

$$\Delta R = \frac{c}{4\Delta f} \qquad (3.56)$$

Here it is assumed that beat frequencies are integer multiples of the modulation frequency, i.e. modulation frequency should be adjusted according to the beat frequency and so to the range. The resolution improvement here comes from the negative slope regions that are not used in ordinary FFT method. However, it is to be noted that the observation tone is now T_m minimum. The difficulty here is to be able to maximize power in the spectrum bins. When the target is at a range where the beat frequency is an integer multiple of the modulation frequency then the corresponding bin will be the bin that holds the maximum power. When this is the case, there is no problem. However, in most of the applications modulation frequency is set to a fixed value ands there are constant bins for different ranges, each of them are corresponding to a target at a different range. When the range of the target does not correspond to any bins, i.e. the beat frequency is not an integer multiple of the modulation frequency, the maximum level of power will not be observed in the spectrum. Instead of a single maximum in the spectrum, the power is distributed to the nearest bins corresponding to the exact range.

This effect is a similar to the effect in FFT, which is known as picket fence effect and will be discussed later in this chapter. When this is the case, the exact range can be estimated from the bins, which holds the maximum powers. Some solution methods for picket fence effect, which can be modified to give an estimation for spectral binning method when the beat frequency is not an integer multiple of the

modulation frequency, will be given in the next chapter after giving information about the FFT processing for FMCW signals.

3.3 Fast Fourier Transform Processing

The optimum detection of a signal in the presence of noise is achieved by using matched filter, in the case of FMCW radar this matched filtering consists of mixing followed by spectrum analysis based on the FFT. This process in the frequency domain is analogous to the use of matched filtering in the time domain for pulse compression radar [12]. Fig. 3.6 shows a sample IF signal output in time domain and Fig. 3.7 shows corresponding frequency spectrum of the signal.

In FFT processing, targets at different ranges appear as different constant frequency components at the mixer output signal. The FFT response of the sinusoidal input reveals a mainlobe and sidelobes, as can be seen in Fig. 3.6 and 3.7. The width of the mainlobe indicates the Fourier domain resolution. The level of the first sidelobe peak relative the mainlobe peak indicates the susceptibility of weak signals to masking by the sidelobes of adjacent strong signals. When using the FFT precautions have to be taken to avoid the problems with aliasing, sidelobe generation and picket fence effect.
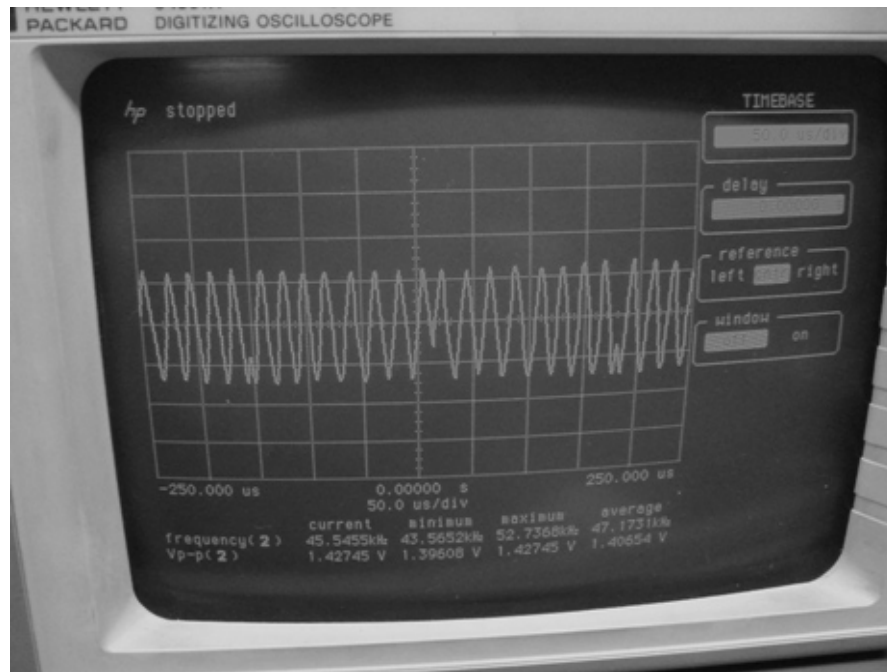
Fig. 3.6 The measured IF signal in time domain
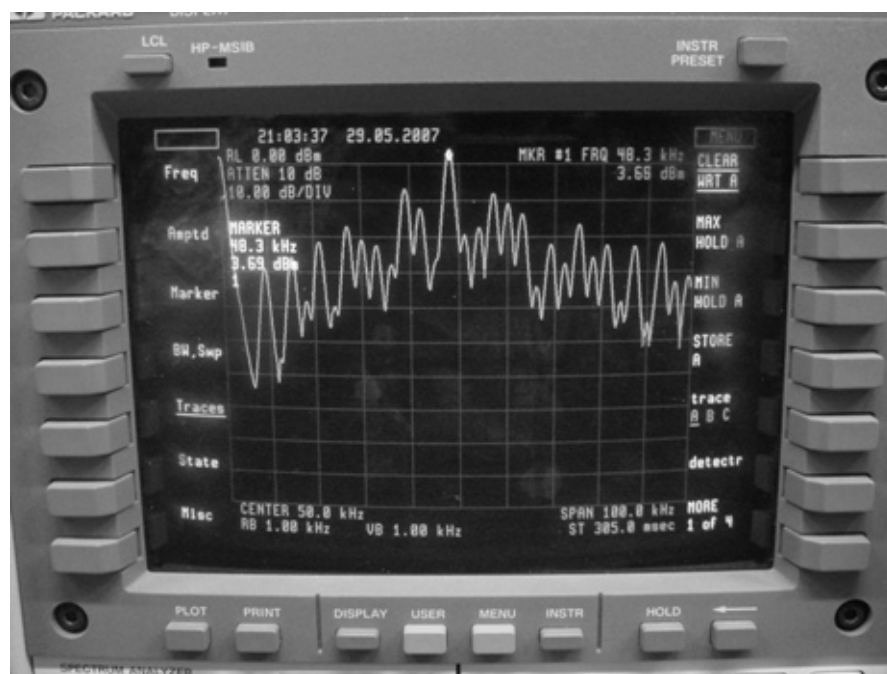
Fig. 3.7 The measured IF signal in frequency domain

3.3.1 Aliasing

Any frequency components in the original spectrum, which extend over half the sampling frequency, overlap in that region and cause aliasing. Because all the values up to the Nyquist frequency are calculated in any case, it is usual to choose a very steep low pass filter with cut off frequency at about 80% of the Nyquist frequency. The low pass filter applied before digitizing must of course be analog. Aliasing is not usually a great problem when analyzing stationary or other signals in affixed frequency band.

3.3.2 Sidelobe Generation

The effect of the time limitation necessary to fit the time signal into a finite record length is known as sidelobe generation, window effect or leakage because the power from the discrete frequency components affects the adjacent bands.

The time windows applied to data effectively determines the filter characteristic associated with the analysis. Applying no special window is the same as applying a rectangular window but for stationary signals and particularly those containing discrete frequency components this is a poor choice of window. A better choice of window function is one which is equal to zero at each end and whose amplitude varies smoothly along the record length. An excellent general-purpose window is known as Hanning. The Hanning window is equivalent to one period of a cosine-squared function. The mainlobe and bandwidth of the Hanning window is greater than the rectangular function but the sidelobes fall off at 60 dB/decade rather than 20 dB/decade.

3.3.3 Picket Fence Effect

The signal spectrum is discretely sampled. Hence, as the name implies it can be considered as the continuous spectrum of the analog signal viewed through the slits in a picket fence. In general, unless a frequency component coincides exactly with an analysis line there will be an error in both the indicated amplitude and

frequency, where the highest line is taken as representing the frequency component.

The loss of apparent amplitude in the FFT when the sinusoid frequency does not correspond exactly to a FFT sample frequency is called as a straddle loss. The straddle loss is a maximum when the sinusoid falls halfway between two FFT frequencies and no window is used. This can be compensated for some degree in FMCW radar by sampling the beat signal non-coherently with the trigger pulse of the sounding signal [13].

As addressed at the end of section 3.2 such a problem similar to the picket fence effect present in the spectral binning method when the beat frequency is not a integer multiple of the modulation frequency. When it is the case then the peak seen in the spectrum is not match with the exact beat frequency corresponding to the range. The actual range can be estimated from the spectrum and a method to solve the picket fence effect is given in the next chapter.

3.3.4 Range Resolution

The ideal range resolution can be calculated as follows:

The FFT will be applied to interval $T_m/2$ therefore total FFT interval is:

$T_f = T_m/2$.

The frequency resolution is:

$$\Delta f_b = \frac{1}{T_f} = \frac{2}{T_m} = 2f_m \qquad (3.57)$$
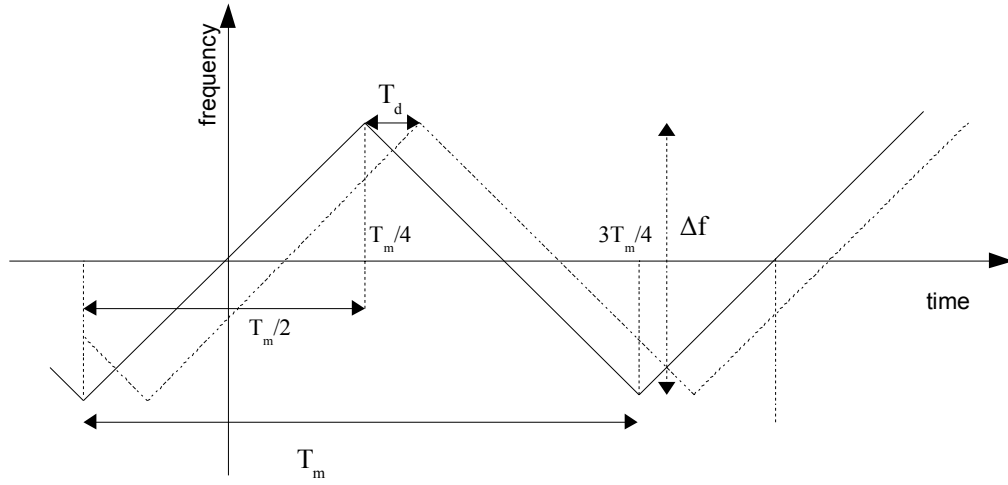
Fig. 3.8 FFT interval illustration for FMCW signal

Recalling (2.5) $f_b = KR$ range resolution can be written as $\Delta R = \dfrac{\Delta f_b}{K}$ and using (3.57) with (2.4) the ideal range resolution for FFT calculated as:

$$\Delta R = \frac{c}{2\Delta f} \tag{3.58}$$

Comparing this range resolution that of (3.56) it is seen that resolution is better for spectral binning. This results from the usage of the negative slope regions that are not used in FFT processing, i.e. the time interval used in spectral binning is T_m instead of $T_m/2$ which is time interval used in the FFT processing. Also from resolution relations (3.58) and (3.56), it is seen that there is a trade off between filter bandwidth, which effects the clutter rejection, and the transient performance, the range resolution.

According to the Nyquist criteria, sampling rate $f_s \geq 2 f_{b,\max}$ recalling (2.5) the sampling rate for maximum range should be:

$$f_s = 2KR_{\max} \tag{3.59}$$

40

The number of samples in FFT interval $N_s = \dfrac{T_f}{T_s} = \dfrac{f_s}{2 f_m}$ here the sampling rate

can be written as:

$$f_s = N_s \cdot 2 f_m \tag{3.60}$$

Equating (3.59) to (3.60) and also using (2.4):

$$N_s = \frac{2 R_{\max}}{\Delta R} \tag{3.61}$$

A trade off between speed and resolution is required because power of two FFT

has computational efficiency proportional to $N_s \log_2 N_s$.

3.4 Non-Fourier Methods

A large number of non-Fourier methods are available for obtaining the frequency domain signal. Time series analysis is an alternative in non-Fourier methods. Time series analysis has been proposed as a method for spectral analysis in the 1970s. A signal is regarded as a realization of a stationary stochastic process. In practice, circumstances may be considered stationary if it is useful to consider the average correlation function or equivalently the power spectrum of the signal over a certain interval. Hence, the signals that can be considered as stationary over a limited time span can also be analyzed with this technique. Time series models have been used in radar signal processing [14], [15].

These methods are more suitable for short bursts of signal than is the Fourier transform. They produce sharper returns without the high sidelobes and fall into general class of maximum entropy spectral estimation methods such as autocorrelation and covariance methods. A digital filter is formed with a transfer function:

$$H(z) = \left[1 - \sum_{n=1}^{p} a_n z^{-n} \right]^{-1} \tag{3.62}$$

The coefficients a_n are selected to produce an impulse response that is the same as the time signal being analyzed. The all-pole (autoregressive) model is used because there is a range of deterministic methods for computing the coefficients to a good approximation. Having evaluated the coefficients it is easy to obtain the filter poles, or to determine the frequency response by evaluating the expression around the unit circle. These methods do have the problem of choosing the best number of coefficients to be used. If too small a number is chosen a poor spectrum will result, if too many coefficients are used then instability and false components can result. The comparison of autocorrelation and covariance techniques with FFT is given in [4].

ARMA models can be used as time series model. ARMA models describe a stationary stochastic process very accurately if the right model structure is used. This renders determination of the model structure a central problem in time series analysis. The model structure is determined by model type, which can be autoregressive (AR), moving average (MA) or auto regressive moving average, and the number of parameters. Often, determination of the model structure using the theoretical considerations is not accurate enough. The theoretical results for the model structure are available for certain types of clutter. However, this model structure will provide inaccurate results when the range cell under consideration contains one or several targets. An algorithm called ARMAsel determines the model structure automatically from the data [16].

3.4.1 The ARMAsel Model

In time series analysis, a signal x is modeled as white noise signal $\in_n$ filtered by a rational or ARMA filter:

$$x_n + a_1 x_{n-1} + \ldots + a_p x_{n-p} = \in_n + b_1 \in_{n-1} + \ldots + b_q \in_{n-q} \quad (3.63)$$

The parameters $a_1, ..., a_p$ are the AR parameters; the number of AR parameters is the AR order p. The parameters $b_1, ..., b_q$ are the MA parameters; the number of MA parameters is the MA order q. the correlation function and the power spectrum can be calculated from the ARMA parameters. A brief notation for (3.63) is:

$$x = \frac{B}{A} \in \qquad (3.64)$$

The roots of the polynomial $A(z) = 1 + a_1 z^{-1} + ... + a_p z^{-p}$ are denoted the poles of the ARMA process. The roots of B(z) are the zeros. Processes are called stationary if all poles are within the unit circle. The ARMA parameters can be used for signal prediction if all zeros are within the unit circle. Three steps are required for the estimation of an ARMA model from N observations of the process x :

1. Type selection: Determination of the model type AR, MA or ARMA

2. Order selection: Determination of model order, the number of parameters

3. Parameter estimation: Determination of model parameters a_i and b_i

In practice, the steps are performed in reverse order. Fist parameter estimation is done for AR models of increasing order $p = 1$ up to $p = L_{\max}$. When the model order is too small to describe the data, a spectral estimate with a small variance and a large bias is obtained. When the model order increase the variance increases. Order selection provides compromise between bias and variance in the estimated spectrum. The order is determined automatically from the data without requiring prior knowledge about the shape of the true spectrum. The steps 3 and 2 are repeated for MA and ARMA models. Finally, the choice between the selected

AR model, the selected MA model, and the selected ARMA models is done with type selection in a similar fashion as order selection.

The ARMAsel algorithm is an algorithm that performs these three steps. All that require as input is the data. The result of the algorithm is a single time series model, which can be used to calculate the power spectrum and the correlation function. Mostly the use of models means usage of a priori knowledge about the shape of the true spectrum. If model assumptions are false, the conclusions draw from the model can be false. In this respect, the ARMAsel algorithm is not dependent on any assumptions regarding the shape of the true spectrum. It provides accurate estimate for a very wide range of spectra.

There are other non-Fourier methods used for FMCW radar signals. Multiple Signal Classification (MUSIC), Prony Method and maximum likelihood estimation (MLE) are the some of the reported used methods brief definitions, comparisons and experimental results of which can be found in [17].

CHAPTER 4

RANGE RESOLUTION IMPROVEMENTS

As given in the previous chapter, there are several methods for FMCW radar IF signal processing all of which are constructed to give time saving in fact real time if possible, good range resolution and cost effective solution. The methods have advantages in some of the aspects as well as disadvantages in some other aspects and can be preferred to the others according to the FMCW radar system specifications and application requirements in which the radar system will be operated.

In this chapter, range resolution improvement methods for previously given signal processing methods will be given and a simple, cost effective solution for our prototype FMCW radar system is explained. First, a fast frequency estimation algorithm (FFEA) based on the FFT technique is explained [18]. Then the picket fence correction method and the possible modification to be used in spectral binning is briefly mentioned.

4.1 The FFEA Method

The conventional FFT method is timesaving, but the precision of the frequency estimation from discrete spectra is limited due to its leakage and picket fence effects as mentioned in previous chapter. In order to improve the measurement precision, some rectification methods for discrete spectra based on FFT, such as zoom FFT, phase difference method, interpolated FFT and energy centrobaric method have been proposed.

The FFEA method based on FFT by combining the predominance of the energy centrobaric method (Hanning window) with the ratio formula method (rectangle window). The drawbacks of the above two methods were overcome by using this kind of algorithm and the measuring precision of target distance was improved. The FFEA is computationally more efficient than MLE, zoom FFT methods, etc. with a computational load of N-point FFT plus a few arithmetic and logic operations. The detailed procedure of the FFEA method is as follows:

1. Establish the corresponding offset threshold δ_0 of the ratio formula method with a rectangle window in certain SNR measuring condition. First, adopt the ratio formula method to estimate the frequency at several points near the peak spectral line after that calculate the root mean square error (RMSE) of these points and find the turning point of RMSE. The offset between the turning point and the peak spectral line was defined as the threshold δ_0.

2. Calculating the N-point FFT of the sampled sequence, the spectrum sequence $S_\omega(k)$ is obtained. Then the spectrum sequence $S_\omega(k)$ is transformed into a new spectrum sequence $S_1(k)$ according to the formula

$$S_1(k) = S_\omega(k) - \frac{1}{2}\left[S_\omega(k-1) + S_\omega(k+1)\right] \qquad (4.1)$$

$k = 0,...,N-1$. This step corresponds to using the Hanning window on the sampled sequence and employing the FFT algorithm. The above transform can be easily realized, which avoids the use of the Hanning window on the sampled data. Calculating the power spectrum $G(k)$ as:

$$G(k) = S_1^2(k)/N \qquad (4.2)$$

the offset δ_1 between the peak spectral line and the actual frequency position can be estimated as:

$$\delta_1 = \frac{\sum\limits_{i=-m}^{m} i \cdot G(k_1 + i)}{\sum\limits_{i=-m}^{m} G(k_1 + i)} \qquad (4.3)$$

where m=3 according to the energy centrobaric method. It is pointed out that in [19] only using several spectra with large power in the mainlobe of G(k) can achieve accurate estimation and m = 3 is suitable.

3. If $|\delta_1| < \delta_0$, the position of the peak spectral line is near to the position of the actual frequency. In this instance the accuracy achieved by using the ratio method with a rectangle window is too low to meet the requirements so the ultimate offset will be established as δ_1. If $|\delta_1| \geq \delta_0$ then the estimation error using the ratio method with a rectangle window will be smaller. Here the offset δ_1 will be established by

$$\delta_1 = \frac{y_{k_1 + 1}}{y_{k_1} + y_{k_1 + 1}} \qquad (4.4)$$

or

$$\delta_1 = -\frac{y_{k_1 - 1}}{y_{k_1} + y_{k_1 - 1}} \qquad (4.5)$$

where y_{k1} is the amplitude of the peak spectral line, $y_{k_1 - 1}$ and $y_{k_1 + 1}$ are the amplitudes of two adjacent spectral lines. The spectral lines in the ratio formula method are shown in Fig. 4.1

4. The estimated beat frequency $\hat{f}_b$ can be calculated as:

$$\hat{f}_b = (k_1 + \delta_1) \cdot \Delta f \qquad (4.6)$$

where k_1 and Δf denote the position of the peak spectral line and the frequency resolution, respectively. Finally, the measured distance R can be calculated using (2.3) using $\hat{f}_b$ instead of f_b.
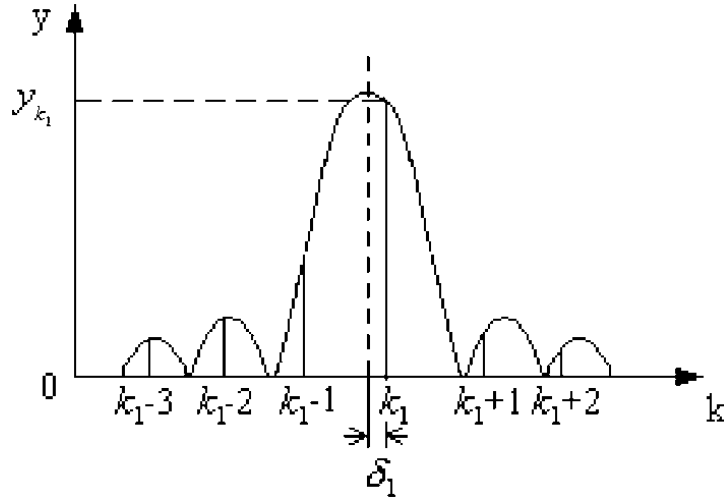
Fig. 4.1 Spectral lines in the ratio formula method

4.2 The Picket Fence Effect Correction

The effect of only measuring the spectrum at discrete frequencies is referred to as the picket fence effect since it is similar to viewing the continuous spectrum measured with a given bandwidth through a picket fence. Therefore, there will be an error in both amplitude and frequency of the highest line in the spectrum of a frequency component. The amplitude error is limited by the ripple in the pass band while the frequency error is limited by the line spacing ΔS of the spectrum. Only in the situation where the frequency component coincides with a centre frequency (line) in the analysis, both the amplitude and the frequency will be correct. This case correspond to the case in spectral binning in which the beat frequency is the integer multiple of the modulation frequency.

48

The most of the methods mainly uses interpolation of the spectrum to solve the problem related with the picket fence effect. If it is assumed that it is a single frequency component, the errors can be compensated for by an interpolation technique on the filter characteristics of the weighting functions [20]. Particularly the frequency correction is important for FMCW radar signals. The frequency correction can be calculated from the difference Δh, in dB, between the highest lines around the peak. The frequency correction ΔS_c Hz for Hanning weighting is given by:

$$\Delta S_c = \frac{2-10\Delta h}{1+10^{\Delta h}} \cdot \Delta S \qquad (4.7)$$

where ΔS is the line spacing of the spectrum. For Hanning weighting, Δh has a maximum of 6 dB that correspond to the situation when the correct frequency coincides with an analysis line. Δh also has a minimum of 0 dB that correspond to the situation when the correct frequency falls exactly between two lines. Table 4.1 shows the frequency correction for Hanning window.

Table 4.1 The frequency compensation for Hanning window

Δh	ΔS_c		Δh	ΔS_c
0,0	0,5		3,0	0,24
0,2	0,48		3,2	0,23
0,4	0,47		3,4	0,21
0,6	0,45		3,6	0,19
0,8	0,43		3,8	0,18
1,0	0,41		4,0	0,16
1,2	0,40		4,2	0,14
1,4	0,38		4,4	0,13
1,6	0,36		4,6	0,11
1,8	0,35		4,8	0,10
2,0	0,33		5,0	0,08
2,2	0,31		5,2	0,06
2,4	0,29		5,4	0,05
2,6	0,28		5,6	0,03
2,8	0,26		5,8	0,02
			6,0	0,00

For rectangular weighting the corresponding frequency correction term is:

$$\Delta S_c = \frac{1}{1+10^{\Delta h}} \cdot \Delta S \qquad (4.8)$$

Using this picket fence correction technique it is possible to achieve a frequency accuracy finer than the line spacing. This method can be modified to be used for spectral binning. By observing the positions and relative amplitudes of the highest spectral lines in the spectrum for different ranges, the relation between relative amplitudes of the highest lines and the actual position of the target can be tabulated. Then comparing the spectrum pattern of the beat signal with these tabulated values by means of a lookup table the effective resolution of the spectral binning method can also be improved further.

A modified version of this correction method for a FMCW radar system implementation is reported. The FMCW radar returns are processed in the spatial domain using FFT processing. In order to provide higher resolution, without an excessive increase in processing time, a modified "picket fence" algorithm is employed. A comparison of experimental results obtained from alternative resolution enhancement techniques is also included. The prototype system operated at 10.5 GHz with a 1 GHz bandwidth [21].

One procedure for reducing the picket-fence effect is to vary the number of points in a time period by adding zeros at the end of the original record, while maintaining the original record intact. This process artificially changes the period, which in turn changes the locations of the spectral lines without altering the continuous form of the original spectrum. In this manner, spectral components originally hidden from view can be shifted to points where they can be observed. Another optimization method to solve the picket fence effect problem and

comparison with zero padding can be found in [22]. In addition, a method called adjustable spectrum can be noted which varies frequency scale by means of adjusting sample rate. This method uses Lagrange interpolation method to proceed the interpolation problem of resample. When sample rate is four times higher than the highest frequency of signal, quite accurate and steady results are obtained [23].

CHAPTER 5

PROTOTYPE SYSTEM AND ZERO CROSSING DETECTOR

5.1 The Prototype FMCW System

The block diagram of the prototype system used in experiments for zero crossing counter measurement evaluation is given in Fig. 5.1. It is very similar to the block diagram given previously for FMCW radar system for one antenna in Chapter 2. In the prototype 10 dB hybrid coupler is used instead of the circulator used in the general case. The 10 dB hybrid coupler usage for this structure is proposed in [24]. The transmitting signal is given to port 1 of the coupler. Port 3 is terminated. The signal flowing through port 4 is used as transmitted signal for mixer and delayed version of the signal coming from the delay line is used as the echo signal. Delay lines of different lengths are used to simulate the radar path. The IF signal from the mixer is fed to the ZCC and beat frequency is determined.
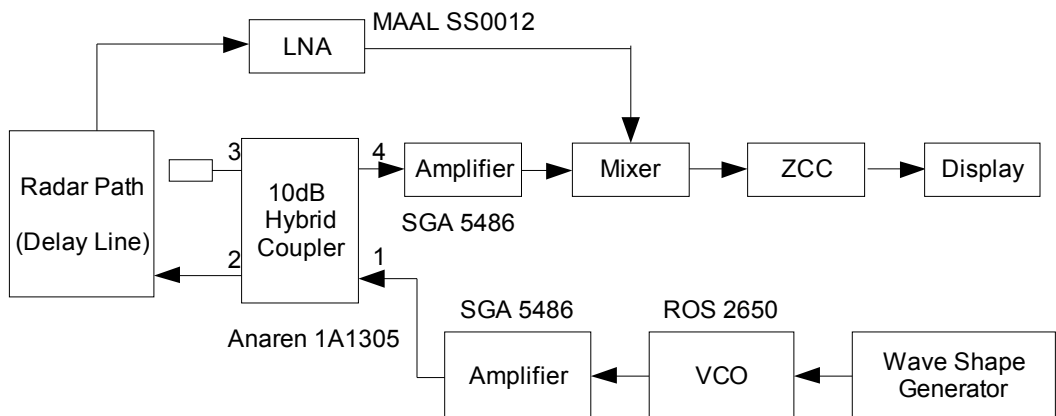
Fig. 5.1 Block diagram for the prototype FMCW radar system

The determined beat frequency is displayed on the display unit and range directly calculated from the beat frequency. Setup is arranged such that both the spectrum analyzer, to be able to see the spectrum of the IF signal, and the oscilloscope, to be able to see the IF signal in time domain, can be fed with the IF signal.
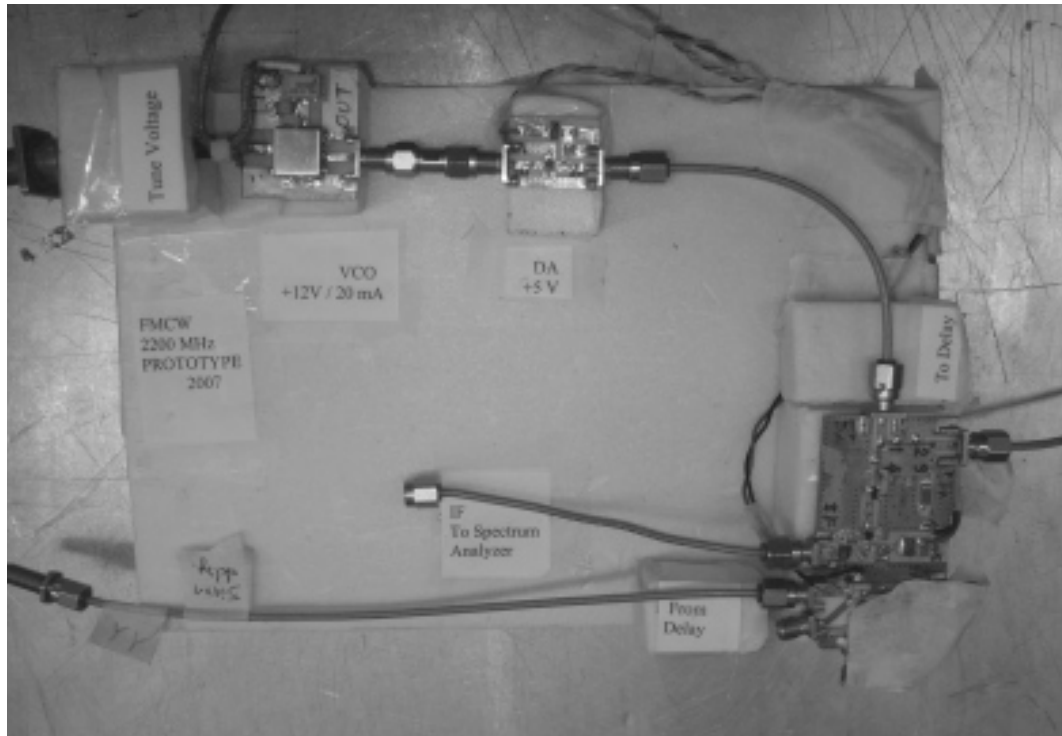
Fig. 5.2 The prototype 2.2 GHz FMCW radar system

5.2 Zero Crossing Counter

Analyzing the IF signal in frequency domain is advantageous for noise suppression and for the low signal to noise ratio (SNR) situations. In the time domain the determination of the IF signal frequency, i.e. the beat frequency, is very difficult for low SNR situations. Nevertheless, when application specification of the FMCW radar is suitable to measure IF signal frequency in time domain, which is the case for the short range applications, then zero crossing

counters (ZCC) can be preferred to determine the beat frequency and consequently the range.

The zero crossing counter is more simple than the signal processing methods both Fourier based and non Fourier methods mentioned in the previous chapter. Therefore, it can be preferred whenever suits the application due to simplicity of the circuitry and the low computational load compared to the other alternatives. In addition, the relatively simple circuitry needed to implement ZCC makes it cost effective solution compared to the other alternatives.

The IF signal frequency is determined by means of counting the zero crossing of the signal for a time interval in the zero crossing detectors. These counters can be implemented in various ways. It is more problematic for high frequencies; if the beat frequencies are not very high then the implementation is simpler. Recalling (2.5) the beat frequency is directly related to range R and the K factor defined in (2.4).

As can be seen in Fig. 5.7 the bins in the spectrum are placed such that the difference between consecutive bins is equal to the modulation frequency, f_m. This means the power distribution of the bins restricted by f_m and so the resolution. However, the ZCC is not strictly limited with this bin placing and can be better for resolution.

Fig. 5.3 shows the block diagram of the zero crossing detector that we used in our prototype system. The high speed comparator used to generate a square wave that has the same frequency with the IF signal. The amplitude of the square wave is adjusted for zero crossing counter to be able to operate. The determined frequency is displayed on the display unit.
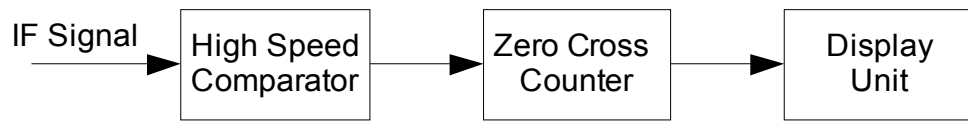
Fig. 5.3 Basic block diagram of zero crossing detector

National Semiconductor high-speed dual comparator LM319 is used to generate square wave. It is also used to provide the well-known Schmitt trigger action for stability. The Schmitt trigger is a comparator, which switches to positive output when the input passes upward through a positive reference voltage. It then uses negative feedback to prevent switching back to the other state until the input passes through a lower threshold voltage, thus stabilizing the switching against rapid triggering by noise as it passes the trigger point. To be able to adjust the reference voltage level 5kΩ variable resistor is used. The Fig. 5.4 shows the schematic of the comparator part.
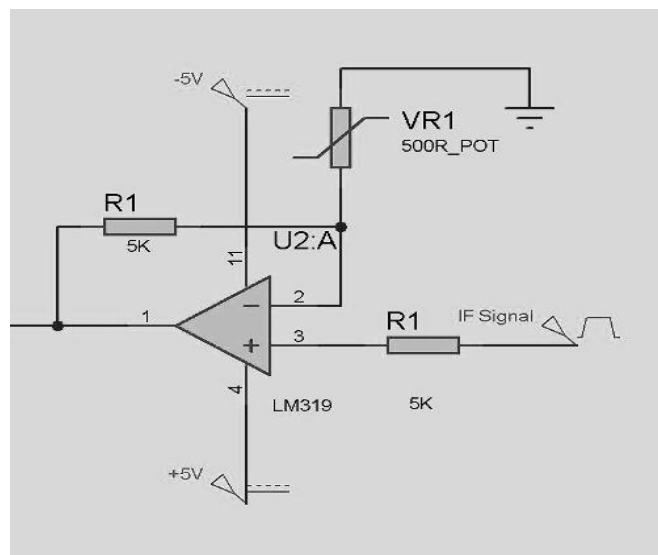
Fig. 5.4 Comparator to generate counting signal from IF signal

Microchip 8-bit CMOS microcontroller PIC 16f877 is used as the zero crossing counter due to availability of the component and the ability to add the future functionality to the detector such as averaging the detected beat frequency to have a more stable measurements, look up tables to increase the range resolution further etc. The output of the comparator is connected to the capture/compare input of the PIC 16f877. The capture/compare interrupt enabled at the rising edge of the counting signal coming from the comparator and timer register content is buffered to calculate the time until next rising edge where another interrupt is enabled. To measure an averaged frequency capture interrupt is configured to be enabled every 4th rising edge. A further averaging is done for the last three reading of the frequency measurement.

Fig. 5.5 The zero crossing counter schematic

The resultant frequency measurement is displayed on a 2x16 alphanumeric liquid crystal display (LCD). The display is also controlled via the PIC 16f877. The code for register settings of the PIC 16f877, frequency calculations and display unit control can be found in Appendix. Fig 5.5 shows the schematic of our zero crossing detector and Fig. 5.6 shows its photograph.
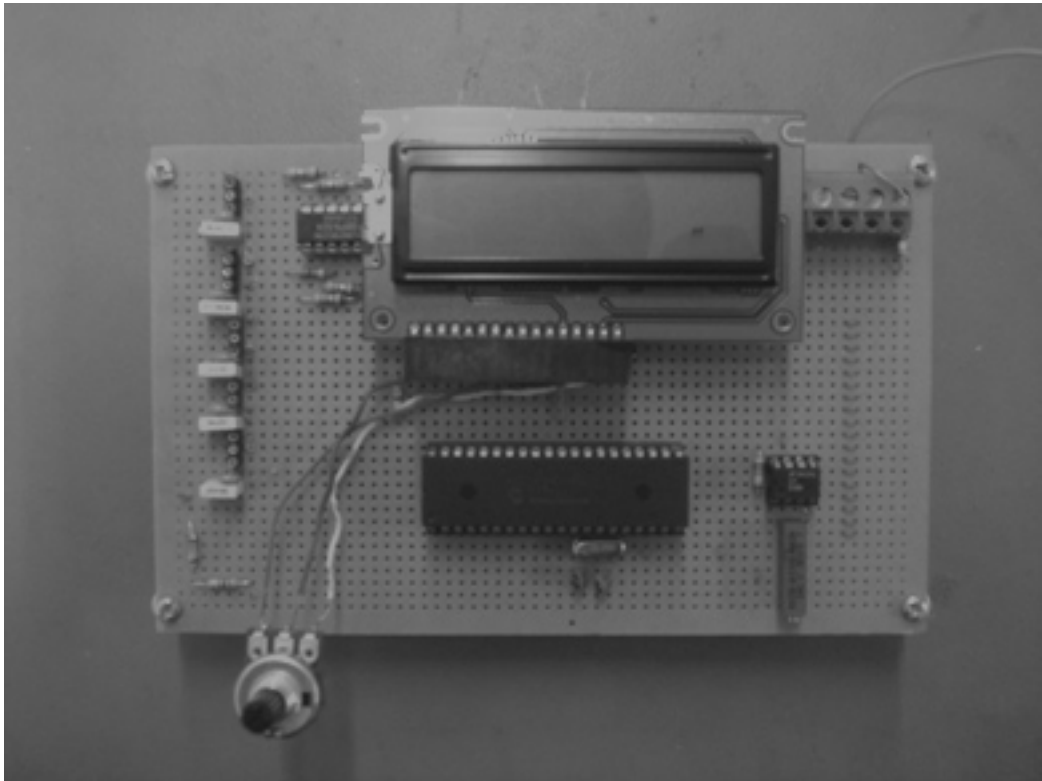
Fig. 5.6 The zero crossing counter circuit

5.3 Experimental Results

The characteristics of the time domain IF signal and the IF signal spectrum are examined for different Δf, the frequency deviation, and f_m, the modulation frequency, values. To be able to observe the effects of each parameter

measurements are done for two groups of four different parameter sets in which one parameter is kept constant while the others change. For the first two sets 76.07 ns delay line is used as the radar path and for the last two sets 69.02 ns delay line is used and for the last four sets 77.07 ns delay line is used. For each set, range resolution limit for FFT and spectral binning is calculated and the zero crossing counter performance is observed. Consecutive readings from LCD are observed and for a number of readings minimum and maximum values are recorded. From these beat frequency readings of zero crossing counter the measured range is calculated and compared with the actual range.

Table 5.1 The measurement results for first group of four sets

	76.07 ns delay (11.41 m)				69.02 ns delay (11.41 m)	
	Set 1.a	Set 1.b	Set 2.a	Set 2.b	Set 3	Set 4
Δf (MHz)	105.8	105.8	92.3	92.3	88.8	132.3
f_m (kHz)	3	2	2	2.53	2.65	2
Bin number	8	8	7	7	6	9
$f_b / 2 f_m$	7.97	7.93	6.95	6.90	5.98	9.08
Measurement errors (m)	-0.11 +0.10	-0.17 +0.14	-0.11 +0.13	-0.20 +0.01	-0.16 +0.04	-0.16 +0.17
Resolution for FFT (m)	1.42	1.42	1.62	1.62	1.70	1.14

5.3.1 The Measurement for Set 1.a

$\Delta f = 105.8 MHz$

$f_m = 3 kHz$

ZCC readings for f_b : 47.8 kHz (min) and 48.7 kHz (max)

Delay line for target path: 76.07 ns

Scope time scale: 50 μs/div, spectrum analyzer scale: 10dB/div
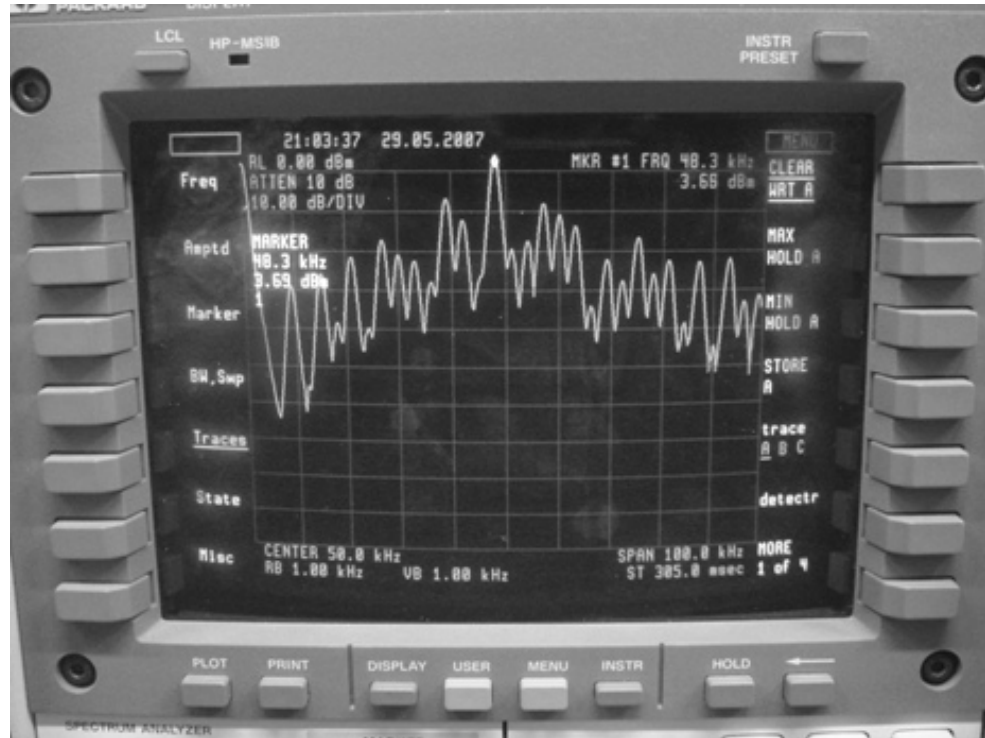
Fig. 5.7 The spectrum of the IF signal for Set 1.a

As seen in Fig. 5.7 the difference between the highest two peaks in the spectrum is about 11 dB and the target at the 16th bin for the spectral binning or at the 8th bin for FFT. This was expected from the ratio $f_b / 2 f_m$ for which the nearest integer is 16.
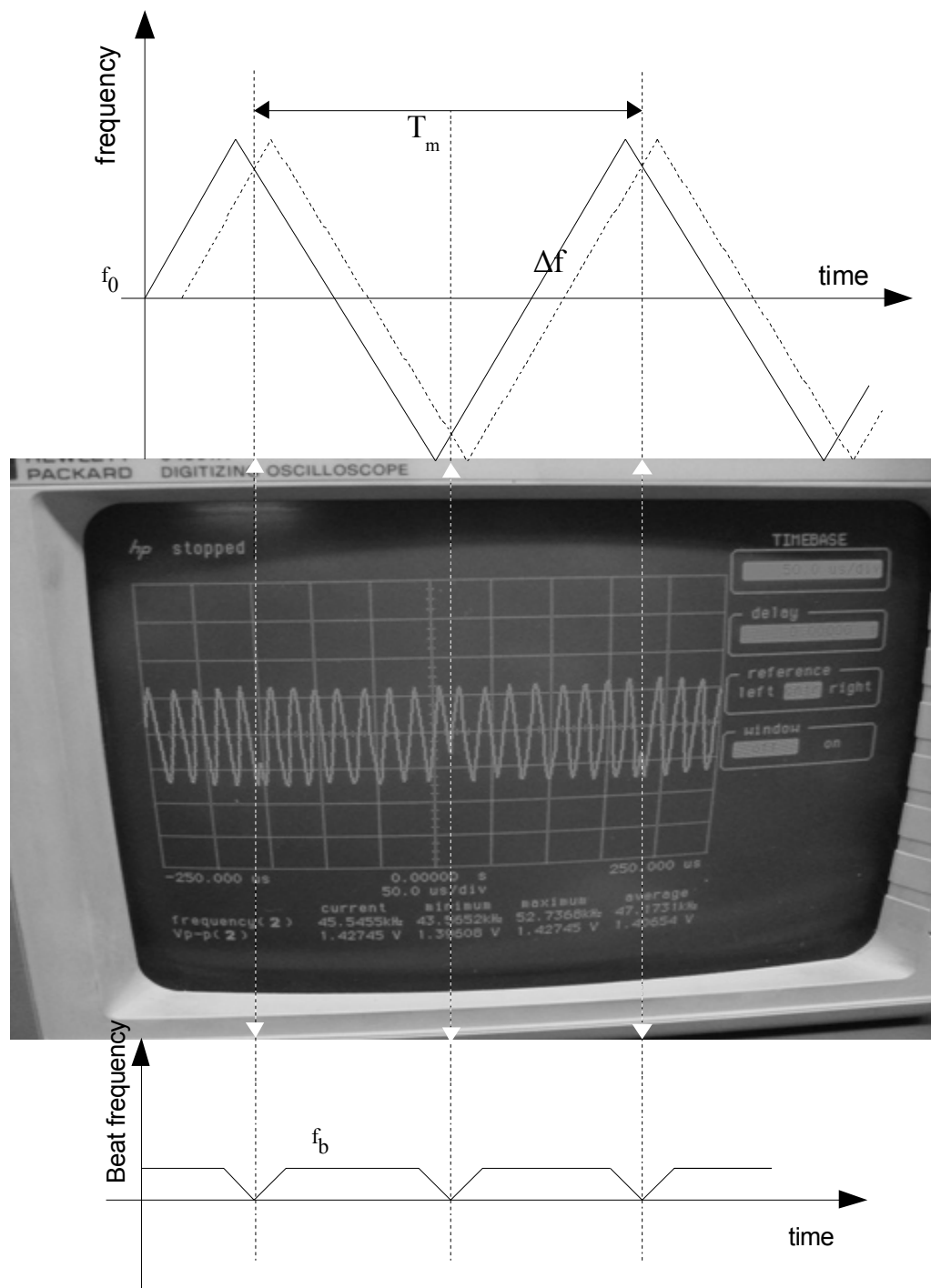
Fig. 5.8 The IF signal in time domain for Set 1.a

In Fig. 5.8, the correspondence between the time domain variation of frequency and the time domain measurement is given in detail for the first measurement set. Similar correspondence can be given for the others. It is seen in Fig 5.8 that cycles between two turn around point are also equal to 8 which corresponds to the bin number, this is true for all the measurement sets, since $T_m/T_b = f_b/f_m$.

The ranges corresponding to the zero crossing counter readings, the actual range and range resolution for spectral binning and for FFT methods are given in Table 5.2.

Table 5.2 The measurement results for Set 1.b

Actual Range	11.41 m
ZCC reading (min)	11.30 m
Error (m)	-0.11
ZCC reading (max)	11.51 m
Error (m)	+0.10
Range Resolution for spectral Binning	0.71 m
Range Resolution for FFT	1.42 m

5.3.2 The Measurement for Set 1.b

$\Delta f = 105.8 MHz$

$f_m = 2 kHz$

ZCC readings for f_b: 31.7 kHz (min) and 32.6 kHz (max)

Delay line for target path: 76.07 ns

Scope time scale: 50 µs/div, spectrum analyzer scale: 10dB/div
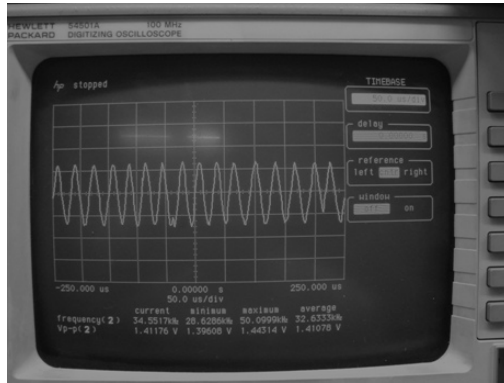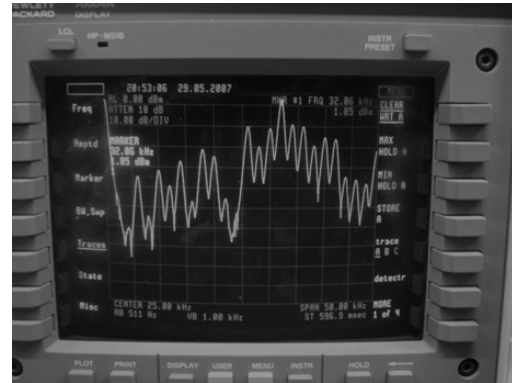
(a)   (b)

Fig. 5.9 The IF signal for set 1.b (a) in time domain (b) in frequency domain

As seen in Fig. 5.9.b the difference between the highest two peaks in the spectrum is about 10 dB. It is also seen that the target at the 16th bin for the spectral binning or the 8th bin for FFT again. Although f_m is changed the bin in the spectrum holding the maximum power did not changed. It is a expected result since the ratio $f_b / 2f_m$ does not dependent on the f_m. Recalling (2.3):

$$f_b / 2f_m = \frac{2\Delta f \cdot R}{c} \tag{5.1}$$

Table 5.3 The measurement results for Set 1.a

Actual Range	11.41 m
ZCC reading (min)	11.24 m
Error (m)	-0.17
ZCC reading (max)	11.55 m
Error (m)	+0.14
Range Resolution for Spectral Binning	0.71 m
Range Resolution for FFT	1.42 m

62

5.3.3 The Measurement for Set 2.a

$\Delta f = 92.3 MHz$

$f_m = 2kHz$

ZCC readings for f_b: 27.8 kHz (min) and 28.4 kHz (max)

Delay line for target path: 76.07 ns

Scope time scale: 100 µs/div, spectrum analyzer scale: 10 dB/div
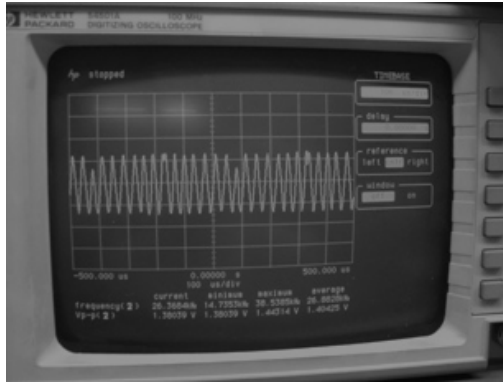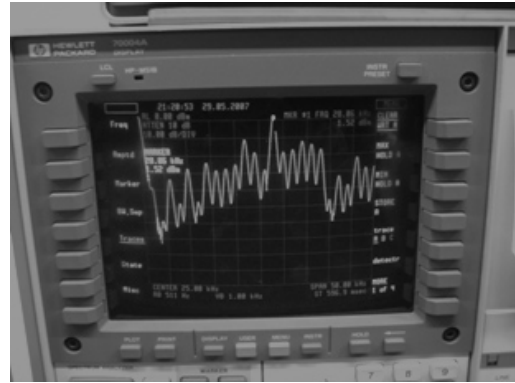
(a)   (b)

Fig. 5.10 The IF signal for set 2.a (a) in time domain (b) in frequency domain

Fig. 5.10.b shows that the difference between the highest two peaks in the spectrum is about 12 dB and the target is at the 14th bin for the Spectral binning or at the 7th bin for FFT. The bin holding the maximum power is different from the Set 1.a and Set 1.b because this time due to change in the frequency deviation Δf, $f_b / 2f_m$ is changed and the nearest integer to the ratio is 14 for this set. Due to change of Δf the range resolution values in Table 5.3 is also changed and the results are tabulated in Table 5.4 as follows:

Table 5.4 The measurement results for Set 2.a

Actual Range	11.41 m
ZCC reading (min)	11.30 m
Error (m)	-0.10
ZCC reading (max)	11.54 m
Error (m)	+0.13
Range Resolution for Spectral Binning	0.81 m
Range Resolution for FFT	1.62 m

5.3.4 The Measurement for Set 2.b

$\Delta f = 92.3 MHz$

$f_m = 2.53 kHz$

ZCC readings for f_b: 34.9 kHz (min) and 35.5 kHz (max)

Delay line for target path: 76.07 ns

Scope time scale: 50 μs/div, spectrum analyzer scale: 10dB/div
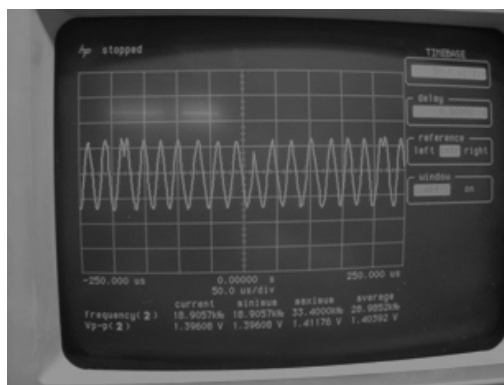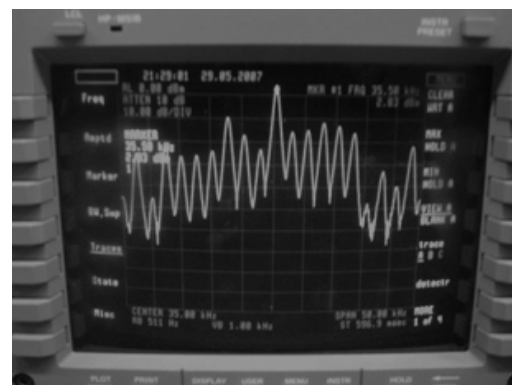
(a)   (b)
Fig. 5.11 The IF signal for Set 2.b (a) in time domain (b) in frequency domain

Fig. 5.11.b shows that the difference between the highest two peaks in the spectrum is about 13 dB and the target at the 14th bin for the Spectral binning or at the 7th bin for FFT. Error in the ZCC measurement is small and this is result of a moderate Δf and 13 dB difference of the highest two peaks.

Table 5.5 The measurement results for Set 2.b

Actual Range	11.41 m
ZCC reading (min)	-0.20 m
Error (m)	1.75
ZCC reading (max)	11.40 m
Error (m)	+0.01
Range Resolution for Spectral Binning	0.81 m
Range Resolution for FFT	1.62 m

5.3.5 The Measurement for Set 3

$\Delta f = 88.8 MHz$

$f_m = 2.65 kHz$

ZCC readings for f_b: 31.7 kHz (min) and 32.1 kHz (max)

Delay line for target path: 69.02 ns

Scope time scale: 50 μs/div, spectrum analyzer scale: 10dB/div
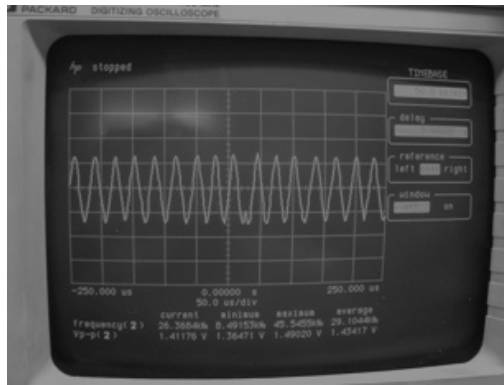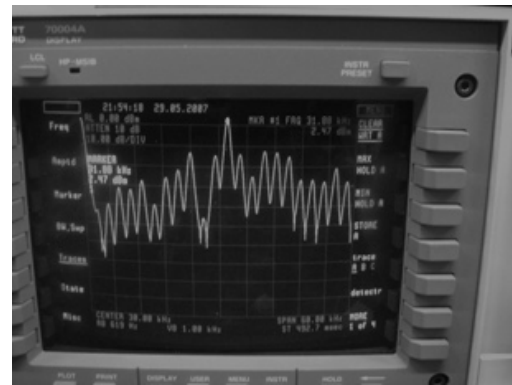
(a)   (b)

Fig. 5.12 The IF signal for set 3 (a) in time domain (b) in frequency domain

The difference between the highest two peaks in the spectrum is about 17 dB and the bin holding the maximum power is 12th bin for the Spectral binning or at the 6th bin for FFT. According to the values of Δf the range resolution values are calculated in Table 5.6. Both the maximum and the minimum readings of ZCC are very accurate as seen in the table; this is a result of relatively high difference in the highest peaks in the spectrum.

Table 5.6 The measurement results for Set 3

|	
Actual Range	10.35 m
ZCC reading (min)	10.19 m
Error (m)	-0.16
ZCC reading (max)	10.31 m
Error (m)	-0.04
Range Resolution for Spectral Binning	0.85 m
Range Resolution for FFT	1.70 m

5.3.6 The Measurement for Set 4

$\Delta f = 132.3 MHz$

$f_m = 2kHz$

ZCC readings for f_b: 36.3 kHz (min) and 37.1 kHz (max)

Delay line for target path: 69.02 ns

Scope time scale: 50 μs/div, spectrum analyzer scale: 10dB/div
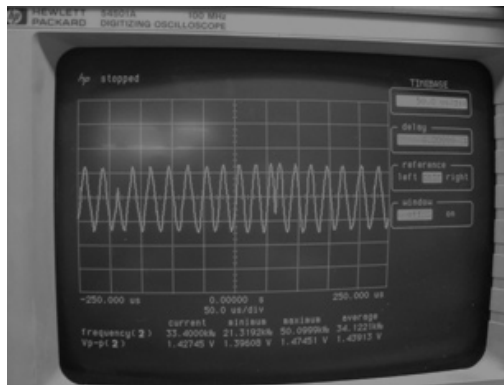
(a)   (b)

Fig. 5.13 The IF signal for set 4.a (a) in time domain (b) in frequency domain

The difference between the highest two peaks in the spectrum is about 10 dB and the bin holding the maximum power is 18th bin for the Spectral binning or at the 9th bin for FFT.

Table 5.7 The measurement results for Set 4

Actual Range	10.35 m
ZCC reading (min)	10.29 m
Error (m)	-0.16
ZCC reading (max)	10.52 m
Error (m)	+0.17
Range Resolution for Spectral Binning	0.57 m
Range Resolution for FFT	1.14 m

In the first groups of sets $f_b / 2f_m$ is very close to integer values corresponding to the bin number holding the maximum power. Therefore, measurements are carried out with another group of sets in which the $f_b / 2f_m$ ratio is not that much close to the integer values.

As seen in Table 5.8, in set 6 and 8 measurement errors are relatively large. For these sets difference of highest peaks are 4 dB and 2.5 dB respectively. For sets 5 and 7 the errors are small where differences are 11 dB and 16 dB respectively.

Bin number of the bin holding maximum power agrees with $f_b / 2f_m$ ratio. This was an expected result from spectral binning analysis. The sets 1-4 and 5-8 are differs from each other for this aspect. In the sets 1-4 target is at ranges that fit to bins, i.e. $f_b / 2f_m$ is close to integer values and difference of the peaks are never worse than 10 dB. This is an expected result from the spectral binning method analysis. In the sets 5-8 target is at ranges that does not fit to bins, i.e. $f_b / 2f_m$ is not close to integer values and difference of the peaks are changes according to the bin power distribution.

Table 5.8 The measurement results for second group of four sets

	77.07 ns delay (11.56 m)			
	Set 5	Set 6	Set 7	Set 8
Δf (MHz)	107.5	102.3	97.3	89.2
f_m (kHz)	2	2	2	2
Bin number	8	8	7	7
$f_b / 2f_m$	8.33	7.63	7.45	6.63
Measurement errors (m)	+0.06 +0.44	-0.38 +0.72	-0.07 +0.08	-0.37 +0.81
Resolution for FFT (m)	1.40	1.46	1.54	1.68
Difference between highest peaks (dB)	11	4	16	2.5

5.3.7 The Measurement for Set 5

ZCC readings for f_b: 33.3 kHz (min) and 34.4 kHz (max)

Delay line for target path: 77.07 ns

Spectrum analyzer scale: 10dB/div

Fig. 5.14 The IF signal for set 5 in frequency domain

$$f_b / 2f_m = 8.33$$

Fig. 5.14 shows that the difference between the highest two peaks in the spectrum is about 11 dB and the target at the 16th bin for the Spectral binning or at the 8th bin for FFT. Error in the ZCC measurement is small and this is result of 11 dB difference of the highest two peaks.

Table 5.9 The measurement results for Set 5

Actual Range	11.56m
ZCC reading (min)	11.61m
Error (m)	+0.06
ZCC reading (max)	12.00m
Error (m)	+0.44
Range Resolution for Spectral Binning	0.70 m
Range Resolution for FFT	1.40 m

5.3.8 The Measurement for Set 6

ZCC readings for f_b: 30.5 kHz (min) and 33.5 kHz (max)

Delay line for target path: 77.07 ns, spectrum analyzer scale: 10dB/div

Fig. 5.15 The IF signal for set 6 in frequency domain

$$f_b / 2 f_m = 7.63$$

Fig. 5.15 shows that the difference between the highest two peaks in the spectrum is about 4 dB and the target at the 16th bin for the Spectral binning or at the 8th bin for FFT. Error in the ZCC measurement is large due to small difference of the highest two peaks.

Table 5.10 The measurement results for Set 6

Actual Range	11.56m
ZCC reading (min)	11.18m
Error (m)	-0.38
ZCC reading (max)	12.28m
Error (m)	+0.72
Range Resolution for Spectral Binning	0.73 m
Range Resolution for FFT	1.46 m

5.3.9 The Measurement for Set 7

ZCC readings for f_b: 29.8 kHz (min) and 30.2 kHz (max)

Delay line for target path: 77.07 ns, Spectrum analyzer scale: 10dB/div

Fig. 5.16 The IF signal for set 7 in frequency domain

$$f_b / 2 f_m = 7.45$$

Fig. 5.16 shows that the difference between the highest two peaks in the spectrum is about 16 dB and the target at the 14th bin for the Spectral binning or at the 7th bin for FFT. Error in the ZCC measurement is very small as seen in below table, due to very large difference of the highest two peaks.

Table 5.11 The measurement results for Set 7

Actual Range	11.56m
ZCC reading (min)	11.49m
Error (m)	-0.07
ZCC reading (max)	11.64m
Error (m)	+0.08
Range Resolution for Spectral Binning	0.77 m
Range Resolution for FFT	1.54 m

5.3.10 The Measurement for Set 8

ZCC readings for f_b: 26.5 kHz (min) and 29.3 kHz (max)

Delay line for target path: 77.07 ns

Spectrum analyzer scale: 10dB/div

$f_b / f_m = 6.63$

Fig. 5.17 shows that the difference between the highest two peaks in the spectrum is about 2.5 dB and the target at the 14th bin for the Spectral binning or at the 7th bin for FFT. Error in the ZCC measurement is large due to small difference of the highest two peaks.

Fig. 5.17 The IF signal for set 8 in frequency domain

Table 5.12 The measurement results for Set 8

Actual Range	11.56m
ZCC reading (min)	11.19m
Error (m)	-0.37
ZCC reading (max)	12.37m
Error (m)	+0.81
Range Resolution for Spectral Binning	0.84 m
Range Resolution for FFT	1.68 m

For the observations of total eight sets of parameters, the following results can be extracted:

- By changing the frequency deviation Δf the pattern of the spectrum, i.e. amplitudes of the spectral bins, place of the bin that holds maximum power etc., are changed.

- The modulation frequency f_m does not change the pattern of the spectrum too much. The effect of changing f_m is to shift the bins to the left and right by decreasing and increasing the modulation frequency, respectively. The amplitudes of the bins in the spectrum are negligibly affected from the changes in f_m.

- When target is at a range that fits to a bin, i.e. $f_b/2f_m$ is close to an integer value, then difference of the peaks are higher than 10 dB and almost all the power is at that specific bin.

- When target is not at a range that fits to bins, i.e. $f_b/2f_m$ is not close to an integer value, then difference of the peaks is not always higher than 10 dB and it changes from case to case.

- Higher the difference between the peak level and the next peak level in the spectrum, more stable the beat frequency reading is. That is, the detection of the range is more accurate.

- When the difference between the peak level and the next peak level in the spectrum is low, ZCC measurements are still acceptable.

- The ZCC measurements are appreciably good for short-range case. It is better when the difference between the peak level and next peak level in the spectrum is high.

In the measurements, ZCC displayed the averaged readings; the sequential readings are close to each other however, there are still some erroneous readings in sequential set of readings. To improve the ZCC performance further, the order statistics can be used to eliminate the erroneous readings. Ordering a set of readings and using the median of these readings as the measured frequency may improve the performance. From the observations during the measurement, it is seen that such a process would improve ZCC reading stability and consequently the range resolution performance.

For a general cycle counter, which measures the number of cycles or half cycles of the beat during the modulation period, the measurement error as given in section 2.3 is formulated in (2.7) as $\delta R = \dfrac{c}{4\Delta f}$.

In our ZCC, beat frequency is calculated just after the second rising edge of the signal instead of counting the zero crossings during the modulation period, T_m. Therefore, range accuracy can be calculated using (2.3) as:

$$\delta R = \frac{c \cdot \delta f_b}{4\Delta f \cdot f_m} \tag{5.2}$$

For our ZCC, frequency is calculated from the counter content (i.e., time) difference of the PIC16F877 for every rising edge hence, the beat frequency is calculated as:

$$f_b = \left(\frac{1}{N \cdot \Delta T} \right) \tag{5.3}$$

where N is the timer content and ΔT is the instruction cycle of PIC, i.e. time between consecutive timer increments. Hence, the frequency accuracy can be calculated for our ZCC as:

$$\delta f_b = \left(\frac{1}{(N+1) \cdot \Delta T} - \frac{1}{N \cdot \Delta T} \right) = \frac{1}{(N+1) \cdot N \cdot \Delta T} = \frac{f_b}{N+1} \tag{5.4}$$

Using (5.4) in (5.2), the range accuracy is calculated as:

$$\delta R = \frac{c \cdot f_b}{4\Delta f \cdot f_m \cdot (N+1)} \tag{5.5}$$

Comparing (5.5) with (2.7) it is seen that the range accuracy is $\dfrac{f_b}{f_m \cdot (N+1)}$ times better for our ZCC than a general cycle counter. The instruction cycle ΔT of

PIC16F877 is 200 ns. Considering the values for f_b and f_m in measurement sets it is seen that our ZCC has a range accuracy at least 6 times better than a general cycle counter and which is at least 12 times better than the range resolution for FFT in (3.58).

Evaluating the measurement results, it can be deduced that ZCC is a good and low cost solution for short-range FMCW radars. In addition, our ZCC is better than common cycle counters for range accuracy. Its main disadvantage is high SNR requirement. For low SNR case zero crossing occurs not only due to the signal itself but also due to the noise. Actually, zero crossing caused by the noise may dominate for some low SNR cases.

ZCC concept could be improved for low SNR case by evaluating the zero crossing patterns and ignoring the non-periodic crossings, the beat frequency can be obtained from the periodic zero crossing patterns. However, to do this, a complex signal processing unit is needed which means complication of the processing. As we can expect there is still a trade off between the complexity and applicable usage areas.

CHAPTER 6

CONCLUSIONS

In this thesis, some of the important aspects of FMCW radar systems are studied. Firstly, brief history of development and contemporary application areas of this type of radars are introduced. Basic working principle of the system is given and the effects of non-ideal properties of the modules used in the system are explained. In addition, the solutions proposed to reduce the effects of these properties preceding this work are investigated in Chapter 2.

In Chapter 3, the signal processing methods used for FMCW radars are explained. The derivation related to a signal processing method called "Spectral Binning" is derived. It is shown that the method can be used for FMCW radar signals and has a better theoretical range resolution compared to ordinary FFT method. After investigating the spectral binning method, FFT method is examined. The important problems in the method and possible solutions are investigated. In addition, the non-Fourier methods are considered and the ARMAsel model, which is used for FMCW radars, is briefly mentioned.

The possible range resolution improvements for these methods are discussed in Chapter 4. These improvement techniques are mainly for Fourier based methods. It is mentioned that since a problem present in spectral binning method that is similar to the picket fence effect present in FFT, the picket fence effect correction technique can be modified to be used for spectral binning method.

After discussing these relatively complex Fourier based and non-Fourier methods a simple signal processing unit, which is suitable for short range FMCW radars, called zero crossing counter is introduced in Chapter 5. A possible zero crossing counter structure is implemented. Parts for this counter are presented to explain the working principle of ZCC. The measurements are done with a prototype FMCW radar and results are discussed for different measurement sets. Measurement sets are prepared to be able to see the performance under different situations. In addition, range accuracy for ZCC is derived and especially second group of measurement sets are prepared to see the relation between the range accuracy of ZCC and range resolution for FFT. From the measurements done with the prototype system it is seen that the ZCC can be used for short range FMCW radars.

Concluding remarks for this thesis about the FMCW radars can be summarized as follows.

The non-ideal properties of FMCW radar modules affect range resolution negatively. The transmitter leakage power is a result of these non-ideal properties and affects the detection of target and measurement of the range for FMCW radars. For the effective usage of the system, the leakage power must be handled carefully. There are pretty good methods such as adaptive reflected power canceller to reduce transmitter leakage power to a negligible level.

The range resolution is also degraded by the non-linear frequency sweep. For high resolution, the non-linearity in the frequency sweep must be corrected and closed loop correction is appreciably successful for the linearization.

The signal processing method is very critical for the range resolution and there is a theoretical limit for it. Most widely used signal processing method is FFT based methods. These methods suffer from some problems like aliasing, sidelobe

generation and picket fence effect. Solutions to aliasing and sidelobe generation problems are generally known and picket fence effect correction can be used to improve the FFT method. In addition, it can be modified to be used in spectral binning. The theoretical range resolution for the spectral binning is two times better than that of FFT processing. Further more, The ARMAsel model is a successful implementation example for non-Fourier FMCW signal processing method.

Although it is very difficult to use ZCC for long-range applications of FMCW radars for which SNR is relatively small, it can be used for short-range FMCW radars as a signal processing unit.

Since spectral lines are placed at the frequencies with a difference equal to the modulation frequency, without corrections spectral methods are restricted to these differences in the spectral lines. However, the ZCC is not strictly limited by the bin spacing and therefore resolution of the ZCC can be better than the other methods for short range FMCW radar applications.

There is a relation between the target range and the power levels of the bins. The difference of the highest peaks in the spectrum is never worse than 10 dB when range fits to a bin. However, there is no such high difference limit for the cases in which range does not fit to any bin. It is seen that, this difference level is important for ZCC performance. Reading performance of ZCC is very good for higher difference levels. In addition, it is still acceptable for lower difference cases.

Our ZCC has a range accuracy at least 6 times better than common cycle counters. Considering all these it can be said that the ZCC is a simple solution compared to both FFT based and non-Fourier solutions due to the simplicity of the implementation. The ZCC is a cost effective solution due to the simplicity of

circuitry needed to implement and ZCC is a good solution for short range FMCW radars.

It can be said that, our prototype system can be improved by implementing a power canceller to reduce the effect of transmitter power leakage. Furthermore, a closed loop correction can be applied for linearization of non-linear frequency sweep. Finally, ZCC performance can be made better by increasing the reading stability by applying order statistics to give the median of a set of consecutive readings.

REFERENCES

[1].   Skolnik, Merrill I.: Introduction to Radar Systems, McGraw-Hill Book Company, 1980 Second Edition.

[2].   Komarov, Igor V., Smolskiy Sergey M.: Fundamentals of Short Range FM Radar, Artech House, 2003.

[3].   Stove, A. G.: Linear FMCW Radar Techniques, IEE Proceedings-F, Vol. 139, No. 5, October 1992.

[4].   Olver A. D., Cuthbert L. G.: FMCW Radar for Hidden Object Detection, IEE Proceedings-F, vol. 135, no. 4, August 1988.

[5].   Brooker, G.M.: Understanding Millimetre Wave FMCW Radars, International Conference on Sensing and Technology, November 2005.

[6].   Beasley P. B., Stove A. G., Reits B. J., As B.-O.: Solving the problems of Single Antenna FMCW Radar, IEEE International Radar Conference, USA, 1990.

[7].   Youngqi J., Guoyu H., Yongbin X., Hui F.: A FTDC Technique to Improve the Range Resolution of Short Range FMCW Radar, 3rd International Conference on Microwave and Millimeter Wave Technology Proceedings, 2002.

[8].   Ahmed N.: Hardware and Software Techniques to Linearize the Frequency Sweep of FMCW Radar for Range Resolution Improvement, 2007.

[9].   William, D.A.: A Highly Linearized mm-Wave Voltage Controlled Oscillator for FMCW Radar Applications, Proc MIOP'88, Microwave Optical Conference, Sindelfingen, 1988.

[10].   Hyung-Gun P., Byungwook K., Young-Soo K.: VCO Nonlinearity Correction Scheme For a Wideband FMCW Radar, John Wiley & Sons, Microwave and Optical Technology Letters, vol. 25, no. 4, 2000.

[11].   Pichler M., Stelzer A., Gulden P., Seisenberger C., Vossiek M.: Frequency Sweep Linearization for FMCW Sensors with High Measurement Rate, IEEE MTT-S International Microwave Symposium, 2005.

[12].   Rabiner R., Gold B.: Theory and Applications of Digital Signal Processing Prentice Hall, New York, 1975.

[13].   Grzywacz A.: Experimental Investigations of Digital Signal Processing Techniques in an FMCW Radar For Naval Application, 14th International Conference on Microwaves Radar and Wireless Communications, MIKON-2002.

[14].   Haykin S., Steinhardt A.: Adaptive Radar Detection and Estimation, J. Wiley and Sons, New York 1992.

[15].   Wensink H., Bazen A.: On Automatic Clutter Identification and Rejection, Radar '99, France1999.

[16].   De Waele S., Broersen P. M. T.: Modeling Radar Data with Time Series Models, European Signal Processing Conference X, EUPSICO 2000.

[17].   Bouchard M., Gingras, D., De Villers Y., Potvin D.: High Resolution Spectrum Estimation of FMCW Radar Signals, IEEE Seventh SP Workshop on Statistical Signal and Array Processing, 1994.

[18].   Liu j., Chen X., Zhang Z.: A Novel Algorithm in the FMCW Microwave Liquid Level Measuring System, Measurement Science and Technology 17 135-138, 2006.

[19].   Ding K., Jiang L.: Energy Centrobaric Correction Method for Discrete Spectrum, Journal of Vibration Engineering 14 354–8, 2001.

[20].   Gade S., Herlufsen H.: Use of Weighting Functions in DFT/FFT Analysis II, Bruel and Kjaer Technical Review, no. 4, pp.1-35, 1987.

[21].   Maskell D. L, Woods G. S., Murray J-M.: A Microprocessor Controlled Microwave Ranging System for High Accuracy Industrial Applications, IEEE Instrumentation and Measurement Technology Conference, IMTC 1994.

[22].   Wu R-C., Tsao P-T.: The Optimization of Spectrum Analysis for Digital Signals, IEEE Transactions on Power Delivery, vol. 18, no. 2, pp. 398-405, April 2003.

[23].   Wu R-C., Tsao P-T.: Theorem and Application of Adjustable Spectrum, IEEE Transactions on Power Delivery, vol. 18, no. 2, p 372-376, April 2003.

[24].   Secmen M., Demir S., Hizal A.: Dual-polarised T/R Antenna System Suitable for FMCW Altimeter Radar Applications, IEE Proceedings Microwaves Antennas and Propagation, October 2006.

APPENDIX

General Features of PIC 16F877

- High performance RISC CPU (35 single word instructions)
- Operating speed: DC - 20 MHz clock input, DC - 200 ns instruction cycle
- Up to 8K x 14 words of FLASH Program Memory,
- Up to 368 x 8 bytes of Data Memory (RAM)
- Up to 256 x 8 bytes of EEPROM Data Memory
- Interrupt capability (up to 14 sources)
- Power-on Reset (POR)
- Power-up Timer (PWRT) and
- Watchdog Timer (WDT) with its own on-chip RC oscillator for reliable operation
- Programmable code protection
- Selectable oscillator options
- CMOS FLASH/EEPROM technology
- Fully static design
- In-Circuit Serial Programming and In-Circuit Debugging via two pins
- Processor read/write access to program memory
- Wide operating voltage range: 2.0V to 5.5V
- Commercial, Industrial and Extended temperature ranges
- Timer0: 8-bit timer/counter with 8-bit prescaler
- Timer1: 16-bit timer/counter with prescaler,
- Timer2: 8-bit timer/counter with 8-bit period register, prescaler and postscaler
- Two Capture, Compare, PWM modules
- 10-bit multi-channel Analog-to-Digital converter

- Synchronous Serial Port (SSP)
- Universal Synchronous Asynchronous Receiver Transmitter (USART/SCI)

Code for PIC 16F877 in ZCC

```
unsigned int temp1, temp2;
unsigned long freq;
unsigned int freqMain;
unsigned char count, timer_count,temp1_count;
void interrupt kes (void)
    {
    di();
    if( TMR1IF)
        {
        timer_count=timer_count+1;
        TMR1IF=0;
        }
    if( CCP1IF )    // capture1 module's flag
        {
        if (count==0)
            {
            temp1 = CCPR1L + 256*CCPR1H;
            temp1_count=timer_count;
            }
        else if (count)
            {
            temp2 = CCPR1L + 256*CCPR1H;
            freq= temp2 - temp1 + 65535*(timer_count-temp1_count);
            timer_count=0;
            }
        count++;
```

```c
        count=count%2;
        CCP1IF = 0;
        }
    ei();
    }


void enab(void)
    {
    RC5=0;
    DelayMs(10);
    RC5=1;
    DelayMs(10);
    RC5=0;
    }


void init(void)        //initialization function for the LCD display, 8 bit, 1 line
    {
    RC3=0;  RC4=0;  DelayMs(50);
    PORTB=0x30;  enab(); DelayMs(20);
    PORTB=0x30;  enab(); DelayMs(20);
    PORTB=0x30;  enab(); DelayMs(20);
    PORTB=0x30;  enab(); DelayMs(20);        //PORTB=0x38; for 2 lines
    PORTB=0x0D;  enab(); DelayMs(20);
    PORTB=0x01;  enab(); DelayMs(20);
    PORTB=0x06;  enab(); DelayMs(20);
    }
void write(char x)     //print function for the LCD
    {
    RC3=1;        RC4=0;
    PORTB=x;    enab();
```

```c
        }
void clr()        // clears the display
        {
        RC3=0;
        RC4=0;
        PORTB=0x01;
        enab();
        DelayMs(20);
        PORTB=0x02;
        enab();
        DelayMs(20);
        }


void UlToStr(char *s, unsigned int bin, unsigned char n)
        {
                unsigned int m;
                s += n;
                *s = '\0';
                while (n--)
                    {
                    m = bin;
                    bin /= 10;
                    *--s = (m - (bin * 10)) + '0';
                    }
        }
void main (void)
        {
        char i;
        char basilan[6];
        timer_count = 0;
```

```
count = 0;
TRISB=0;              // portB output
TRISC=0x04;           // RC2 input, others output
PIE1=0x05;            // enable timer1 & ccp1 interrupt
T1CON=0x21;           // timer1 on, 1:4 prescale
CCP1CON=0x06;         // capture every 4th rising edge
init();
ei();              // enable interrupts global & peripheral
        for(;;)
        {
                if (count == 0)
                        {
                        di();
                        count=0;
                        timer_count=0;
                        temp1_count=0;
                        TMR1H=0;
                        TMR1L=0;
                        freqMain=5000000/freq;       //@20 MHz
                        UlToStr(basilan, freqMain, 5);
                                for(i=0; i<5; i++)
                                write(basilan[i]);
                                DelayMs(200);
                        clr();
                        init();
                        ei();
                        }
        }
}
```